

1 **Adenylate cyclase activity of TIR1/AFB auxin receptors for root**
2 **growth**

3

4 **Authors:** Linlin Qi¹, Mateusz Kwiatkowski², Huihuang Chen¹, Lukas Hoermayer¹, Scott
5 Sinclair¹, Minxia Zou¹, Charo I. del Genio³, Martin F. Kubeš⁴, Richard Napier⁴, Krzysztof
6 Jaworski², Jiří Friml^{1,*}

7

8

9 **Affiliations:**

10 ¹Institute of Science and Technology Austria (ISTA) – 3400 Klosterneuburg (Austria).

11 ²Department of Plant Physiology and Biotechnology, Nicolaus Copernicus University in
12 Toruń – 87-100 Toruń (Poland).

13 ³Centre for Fluid and Complex Systems, Coventry University – CV1 5FB Coventry (United
14 Kingdom).

15 ⁴School of Life Sciences, University of Warwick – CV4 7AL Coventry (United Kingdom).

16

17

18 * Correspondence to: jiri.friml@ist.ac.at

19

20

21 **Abstract**

22 **Phytohormone auxin acts as major coordinative signal in plant development mediating**
23 **transcriptional reprogramming by a well-established canonical signalling pathway:**
24 **TIR1/AFB auxin receptors are F-box subunits of ubiquitin ligase complexes; in response**
25 **to auxin they associate with Aux/IAA transcriptional repressors and by ubiquitination**
26 **destine them for degradation. Here we identified adenylate cyclase (AC) activity as an**
27 **additional functionality of TIR1/AFBs across land plants. Auxin together with Aux/IAAs**
28 **stimulates cAMP production by TIR1/AFBs representing a novel signalling output from**
29 **the TIR1/AFB-Aux/IAA co-receptor complex. Three separate mutations in the AC motif**
30 **of the TIR1 C-terminal region, which all abolish the AC activity, render TIR1 ineffective**
31 **in mediating gravitropism, auxin-induced root growth inhibition and partly compromise**
32 **auxin-induced transcription. These discoveries highlight an importance of TIR1/AFB AC**
33 **activity in auxin signalling. They also identify a unique phytohormone receptor cassette**
34 **combining F-box and AC motifs, and new possibilities for cAMP as a second messenger**
35 **in plants.**

36

37 **Main**

38 Auxin is the major endogenous regulator of growth and development¹. Earlier genetic screens
39 based on auxin-induced root growth inhibition have identified major components of auxin
40 signalling^{2,3}. Further assisted by biochemical analysis, this established the core outline of the
41 canonical auxin signalling pathway with TIR1/AFBs acting as auxin receptors. The sole
42 proposed biochemical function of TIR1/AFBs is their action as F-box proteins, the subunits
43 determining the substrate specificity of the SCF-type E3 ubiquitin ligase complex^{4,5}. Auxin
44 binding to the pocket of TIR1 increases the affinity between TIR1 and the Aux/IAA repressors,

45 promoting the ubiquitination and subsequent degradation of Aux/IAs, thus releasing their
46 repression on ARF-mediated transcription⁵⁻⁸. This nuclear mechanism explains how auxin can
47 modulate transcription, and has stood the test of time for more than 15 years. However, several
48 members of the TIR1/AFB family especially AFB1 are also present in cytosol⁹, and recent
49 accumulating observations suggest the existence of a non-transcriptional responses
50 downstream of TIR1/AFBs^{10,11}. Root growth inhibition strictly depends on functional
51 TIR1/AFBs, but is very rapid and reversible¹². It involves auxin-induced apoplast alkalinisation
52 and membrane depolarization^{13,14}. A member of the cyclic nucleotide-gated channel family
53 (CNGC) CNGC14 is essential for auxin-induced cytosolic calcium (Ca²⁺) transients and
54 partially responsible for apoplast alkalinisation. These Ca²⁺ transients were originally proposed
55 to be triggered by unknown cell surface auxin receptors¹⁵, but later the CNGC14-Ca²⁺ pathway
56 was placed downstream of TIR1/AFBs signalling in root hairs¹⁶. All of the above collectively
57 suggests that TIR1/AFBs drive a non-transcriptional signalling activity, for which the
58 underlying molecular mechanism remains a mystery. Hence, the molecular functions of
59 TIR1/AFBs are still not fully elucidated.

60 Here we demonstrate that TIR1/AFB auxin receptors have adenylylase (AC) activity,
61 which is important for its physiological function in root growth regulation. This provides an
62 unexpected twist to the mechanism of TIR1/AFB-mediated auxin signalling, and suggests
63 cAMP as a second messenger in this key signalling mechanism in plants.

64

65 **TIR1/AFBs auxin receptors have adenylylase activity**

66 The existence of an uncharacterized branch of TIR1/AFB signalling for root growth
67 regulation¹¹ prompted us to search potential additional roles of TIR1/AFB auxin receptors by
68 analysing their sequences.

69 Putative motifs for AC activities in plants have been identified by examining conserved
70 sequences of reported AC proteins^{17,18}. Screening the TIR1/AFBs protein sequences, we found
71 a relatively conserved, possible AC motif in the unannotated C-terminal region (Fig. 1a)
72 suggesting an AC activity of TIR1/AFB auxin receptors.

73 An *E. coli* complementation assay has been widely used to evaluate the AC activity of
74 potential candidates, in which an AC-deficient strain (SP850) is complemented by genes of
75 interest. Those possessing AC activity will produce cAMP, which can activate the lactose
76 operon and change the colour of MacConkey agar to red¹⁹. We tested all 6 TIR1/AFBs with
77 this assay, using a characterized AC (HpAC1) as a positive control¹⁹. Only AFB1 and AFB5
78 proteins can be detected by Western blot and those receptors also showed clear AC activity
79 similar to HpAC1 (Extended Data Fig. 1a,b). Due to lack of detectable protein, the AC activity
80 of the other 4 TIR1/AFBs could not be assessed. To further confirm AC activity, we purified
81 GST-AFB5 protein from *E. coli* (Extended Data Fig. 2a), and performed an AC activity assay
82 using the Enzyme Immunoassay Kit to detect cAMP. This revealed a clear AC activity of GST-
83 AFB5, with a preference for Mn²⁺ as cofactor (Fig. 1b). To validate these results, we analysed
84 the enzyme kinetics of GST-AFB5 by detection of cAMP with a more sensitive LC-MS/MS
85 method. As shown in the LC-MS/MS spectrum, cAMP was reliably detected in the reaction
86 system (Fig. 1c). The Michaelis-Menten kinetics identified a $V_{\max} = 10.45$ fmol/min/ μ g and
87 $K_M = 0.675$ mM for GST-AFB5 (Fig. 1d), which is comparable to other reported plant ACs²⁰⁻
88 ²³. Similarly, we also determined the AC enzyme kinetics for GST-AFB1 purified from *E. coli*
89 (Extended Data Fig. 1c and Extended Data Fig. 2b). To test whether those members showing
90 negative results in the *E. coli* complementation assay also have AC activity, we purified the
91 His-GFP-FLAG-TIR1 protein from *Sf9* insect cells (Extended Data Fig. 2c). We performed
92 similar enzyme kinetics assay and identified a $V_{\max} = 7.462$ fmol/min/ μ g and $K_M = 0.644$ mM
93 for TIR1 (Fig. 1e and Extended Data Fig. 1d).

94 Comparison of orthologous sequences from the moss *Physcomitrella patens* revealed that
95 the AC motif in the C-terminal of TIR1/AFBs is also conserved in this early diverging land
96 plant (Extended Data Fig. 3a). We purified all 4 PpAFBs from *E.coli* (Extended Data Fig. 2d-
97 g) and confirmed their AC activity (Extended Data Fig. 3b), showing that the TIR1/AFBs AC
98 activity had already evolved in early ancestral land plants.

99 In summary, we demonstrated by three independent methods that TIR1, AFB1 and AFB5
100 possess AC activity, and given the conservation of the AC motif, it is likely that all 6
101 Arabidopsis TIR1/AFBs have AC activity. Moreover, the AC activity detected in the moss
102 AFBs shows that it is a common feature also in the early diverging land plants.

103

104 **A conserved C-terminal motif is responsible for the AC activity**

105 The reported core AC motif [RKS]X[DE]X{9,11}[KR]X{1,3}[DE] contains 4 functionally
106 assigned residues (Fig. 1a). [RKS] in position 1 allows hydrogen binding with adenine, [DE]
107 in position 3 confers substrate specificity for ATP, [KR] stabilizes the transition state from
108 ATP to cAMP, and the final [DE] residue is the cofactor Mg²⁺/Mn²⁺ binding site¹⁷. Among the
109 C-terminal AC motifs of TIR1/AFBs, the last 3 residues are highly conserved and strictly fit
110 the original core motif, but the first residue is more relaxed, with only AFB2 and AFB3 having
111 a perfectly matched motif. The demonstration of AC activity for TIR1, AFB1 and AFB5
112 extends the first residue from the original [RKS] to [RKSPY], so that all the 6 TIR1/AFBs have
113 this extended AC motif in the C-terminal (Fig. 1a) suggesting that this motif is responsible for
114 the AC activity.

115 To test this, we mutated separately the last 3 conserved residues in the C-terminal AC motif
116 of AFB5 to alanine (m1, m2, m3 in Fig. 1a), and performed the *E. coli* complementation assay.
117 The results showed that, while the mutated proteins expressed comparably to the wild-type

118 AFB5, all 3 mutated AFB5 variants lost their AC activity (Fig. 2a). To further confirm this, we
119 purified the mutated GST-AFB5 from *E. coli* (Extended Data Fig. 2h) and performed the AC
120 activity assay. Indeed, all mutated variants lost the AC activity except AFB5^{ACm2}, which
121 maintained a very weak activity (Fig. 2b). Full-length TIR1 was unstable in the *E. coli*
122 expression system, but we managed to purify an N-terminal deleted version (TIR1^{ΔNT})
123 (Extended Data Fig. 2i), which still retains AC activity. We mutated the same 3 residues to
124 alanine in the TIR1^{ΔNT} and purified them from *E. coli* (Extended Data Fig. 2j). Results from
125 the AC activity assay clearly demonstrate that again all 3 mutations abolished the AC activity
126 of TIR1^{ΔNT} (Fig. 2c).

127 To test whether these mutations interfere with auxin perception and the first step of the
128 canonical pathway – the auxin induced TIR1/AFB interaction with Aux/IAAs, we introduced
129 the same mutations into the full length TIR1. The pull-down reactions in presence of IAA with
130 *in vitro* translated full length TIR1-HA and purified GST-IAA7 showed that while the ACm2
131 mutation abolished the interaction between TIR1^{ACm2} and IAA7, the ACm1 and ACm3
132 mutations did not have effects (Fig. 2d). This shows that the AC activity and Aux/IAA
133 interaction capability can be uncoupled by ACm1 and ACm3 mutations in the AC motif.

134 Together, these results prove that the conserved C-terminal AC motif is responsible for the
135 AC activity of TIR1/AFBs and can be mutated to selectively abolish this activity.

136

137 **Auxin in conjunction with Aux/IAAs stimulate TIR1/AFB AC activity**

138 Next, we tested whether auxin perception by TIR1/AFB has any effect on AC activity.
139 According to the published crystal structure of TIR1, the C-terminus forms a cap structure,
140 which closes the solenoid of leucine-rich repeats⁸. Spatially, the auxin binding pocket is located

141 close to the AC motif (Extended Data Fig. 4a), suggesting there may be mutual communication
142 between the AC activity, auxin binding and auxin-triggered Aux/IAA interaction.

143 To gain additional insight into this issue, we docked the structure of ATP to the TIR1-IAA-
144 Aux/IAA complex⁸. This shows that the orientation of ATP molecule, with the adenyl head
145 close to the beginning of the AC domain (in magenta), the sugar moiety in direct contact with
146 E554 (ACm1 in Fig. 1a), and the phosphate groups next to a positively charged residue R555,
147 fits plausibly into the structure of the TIR1-IAA-Aux/IAA complex. However, the remaining
148 half of the AC motif including the two amino acids we mutated before R566 (ACm2) and D568
149 (ACm3) is on the other side of the TIR1 surface without a direct predicted contact with the
150 docked ATP (Fig. 3a and Extended Data Fig. 4b). It is possible that the crystalized structure
151 does not reflect the genuine structure *in planta*, or that ATP binding causes conformational
152 change. Importantly, V84 from the Aux/IAA degron constrains space available to ATP,
153 possibly reducing its mobility and thus increasing the reaction efficiency (Fig. 3a). This
154 structural perspective suggests that the auxin-triggered association between Aux/IAs and
155 TIR/AFBs may enhance their AC activity.

156 To test this, we purified AFB5, along with the IAA7 and IAA17 co-receptors from *E. coli*
157 with GST tags cleaved (Extended Data Fig. 2k-m) and performed *in vitro* AC activity assays
158 for AFB5 in the presence of 10 μ M IAA, IAA7 or IAA17, and their combinations. The results
159 showed that IAA or IAA7/17 alone did not have any significant effect on the AFB5 AC activity.
160 However, IAA together with IAA7 or IAA17 significantly enhanced the AC activity, with
161 IAA7 showing a stronger effect than IAA17 (Extended Data Fig. 5). To confirm this
162 observation, we did similar experiment with His-GFP-FLAG-TIR1 protein purified from *Sf9*
163 insect cells. Again, significant increase in TIR1 AC activity was observed in the presence of
164 IAA together with IAA7 or IAA17 (Fig. 3b). These results show that the IAA-induced
165 assembly of the TIR1-Aux/IAA complex enhances the AC activity.

166 Next, we tested whether stimulation of TIR1/AFB AC activity can be detected *in planta*.
167 We treated Col-0 seedlings with 100 nM IAA and harvested roots at different time points to
168 measure cAMP level using LC-MS/MS. Indeed, after an initial slight depletion of cAMP, IAA
169 treatment led to a steady increase of cAMP levels after 1 h (Fig. 3c). Whilst only the difference
170 at 6 h is statistically significant, this dynamic trend was reproducible in multiple repetitions.
171 Considering that TIR1/AFBs are not the only ACs in *Arabidopsis* and the list of AC enzymes
172 is growing continuously^{17,18}, and that cAMP signalling is likely highly compartmentalized²⁴
173 leading to a very localized increase of cAMP levels around the TIR1/AFBs receptors
174 themselves, the activation effect will be predictably underestimated by measuring entire root
175 cAMP content. Hence, the detected differences, whilst small in whole root tissue, are likely
176 physiologically relevant. Notably, the increase of cAMP levels after auxin treatment was
177 completely abolished in *tir1-1 afb2-1 afb3-1* (*tir* triple) mutant, and even values for both Mock
178 and IAA in *tir* triple were slightly lower comparing to the Mock value of Col-0 (Fig. 3d).
179 Collectively, these data indicate that auxin treatment increases cAMP level in roots through
180 TIR1/AFBs.

181 Collectively, these data show that the auxin-induced interaction between TIR1/AFBs and
182 Aux/IAAs stimulates the AC activity consistent with auxin-triggered cAMP increase in roots.
183 This represents a novel molecular output of TIR1/AFBs, distinct from their E3 ligase activity.

184

185 **TIR1 AC activity is crucial for root growth inhibition and root gravitropism**

186 To evaluate the importance of the AC activity to the physiological function of TIR1 *in planta*,
187 we tested the ability of TIR1^{ACm1-3} protein variants to mediate root growth regulation by
188 introducing the *pTIR1::TIR1^{ACm1-3}* constructs into *tir1-1 afb2-3* double mutant. As shown
189 before²⁵, root growth was strongly inhibited when Col-0 seedlings were grown on plates

190 containing 100 nM IAA, while *tir1-1 afb2-3* was completely resistant under these conditions.
191 The *pTIR1::TIR1* almost fully complemented this mutant phenotype, whereas all 3 mutated
192 *pTIR1::TIR1^{ACm1-3}* variants showed compromised complementation (Fig. 4a,b). Notably, the
193 *TIR1^{ACm2}* mutation, which also abolishes the interaction with Aux/IAAs (see Fig. 2d), rendered
194 *TIR1* completely non-functional. Overall, this shows that AC activity is crucial for the *TIR1*-
195 mediated root growth inhibition by auxin.

196 To further confirm this notion, we used the synthetic biology tool, the engineered *cvxIAA*-
197 *ccvTIR1* pair system²⁶. As illustrated (Fig. 4c), natural IAA can only bind *TIR1* to trigger root
198 growth inhibition but not the *ccvTIR1* with the engineered auxin binding site and vice versa,
199 the auxin analogue *cvxIAA* binds and activates only *ccvTIR1* but not the *TIR1* or AFBs.
200 Therefore, *pTIR1::TIR1*, *pTIR1::ccvTIR1* and the 3 corresponding mutated
201 *pTIR1::ccvTIR1^{ACm1-3}* constructs were generated and transformed into the *tir1-1 afb2-3*
202 background. Consistent to the previous reports²⁶, *cvxIAA* (500 nM) cannot trigger root growth
203 inhibition in the absence of the engineered *ccvTIR1*, but triggers strong root growth inhibition
204 in the *ccvTIR1* transgenic plants. Again *ccvTIR1^{ACm2}* showed a complete resistance (Fig. 4d) in
205 line with its additional inability to interact with Aux/IAAs (see Fig. 2d), whereas in *ccvTIR1^{ACm1}*
206 as well as *ccvTIR1^{ACm3}* lines also almost no root growth inhibition was observed (Fig. 4d). This
207 confirms that *TIR1* AC activity is essential for *TIR1*'s role in mediating root growth inhibition
208 by auxin.

209 Auxin effect on root growth underlies positive root gravitropism²⁷. To test whether *TIR1*
210 AC activity is also required for root gravitropism, we analysed the dynamics of gravitropic root
211 bending angle in the *pTIR1::TIR1* and *pTIR1::TIR1^{ACm1/3}* complemented lines. *tir1-1 afb2-3*
212 has clear defects in root gravitropic response comparing to Col-0. *pTIR1::TIR1* largely
213 complemented the gravitropic defects of *tir1-1 afb2-3*, while *TIR1^{ACm1}* and *TIR1^{ACm3}* showed

214 only very slight complementation (Fig. 4e). This result proves that AC activity of TIR1 is also
215 required for root gravitropism.

216 These genetic experiments collectively show that AC activity is crucial for TIR1 function
217 in auxin-induced root growth inhibition and root gravitropism *in planta*.

218

219 **TIR1 AC activity is not essential for rapid auxin effects in roots**

220 To understand the temporal dynamics of the importance of AC activity for root growth
221 regulation by auxin, we evaluated the root growth kinetics of *pTIR1::ccvTIR1* and
222 *pTIR1::ccvTIR1^{ACm1}* lines using vRootchip in combination with vertical microscopy^{12,13}.
223 cvxIAA application gradually inhibited root growth in both lines, but no significant difference
224 was observed between them within the 1st hour (Extended Data Fig. 6a). Then we followed the
225 root growth dynamics with a vertical scanner finding that the resistance of *pTIR1::ccvTIR1^{ACm1}*
226 to cvxIAA-induced root growth inhibition occurs only after 1 h (Extended Data Fig. 6b)
227 correlating with the dynamics of the auxin-induced increase of cAMP level in root (see Fig.
228 3c). This suggests that TIR1 AC activity is required for root growth regulation only at later
229 stages.

230 It has been demonstrated previously that auxin-induced rapid root growth inhibition is
231 closely related to Ca²⁺ signalling and apoplast alkalinisation^{13,15}. To clarify whether TIR1 AC
232 activity is required for these rapid non-transcriptional responses, we monitored the cytosolic
233 Ca²⁺ spikes and apoplast alkalinisation in the AC motif-mutated *TIR1* transgenic lines. cvxIAA
234 triggers similar cytosolic Ca²⁺ increase in *ccvTIR1* and *ccvTIR1^{ACm1}* lines within 1 min, and
235 there is also no significant difference for IAA-induced apoplastic pH increase in *TIR1* and
236 *TIR1^{ACm1}* lines (Extended Data Fig. 7a,b).

237 Together, these observations indicate that TIR1 AC activity, despite being crucial for the
238 sustained auxin-induced root growth inhibition, is not essential for rapid auxin effect on root
239 growth and associated rapid apoplast alkalinisation and Ca²⁺ transients.

240

241 **TIR1 AC activity contributes to the auxin-induced transcriptional regulation**

242 Since the TIR1 AC activity seems to be important only for a long-term auxin effects on root
243 growth and gravitropism, which are likely involving transcriptional regulation, we tested auxin
244 effect on transcription of selected auxin responsive genes using quantitative real-time PCR
245 (qRT-PCR). Consistent with previous results²⁶, cvxIAA specifically activates the transcription
246 of the selected auxin-responsive genes including *GH3.3*, *GH3.5*, *IAA5*, *IAA19* and *LBD29* in
247 *ccvTIR1*, but not in control *TIR1* line. Indeed, the transcriptional upregulation of these genes is
248 notably reduced in *ccvTIR^{ACml}* (Fig. 4f-j), suggesting that TIR1 AC activity also contributes to
249 auxin-induced transcriptional regulation.

250

251 **Conclusions**

252 The current framework of canonical auxin signalling relies on TIR1/AFB auxin receptors
253 acting as F-box proteins, which form a functional SCF-type E3 ubiquitin ligase together with
254 other subunits⁴⁻⁷. Here we show that TIR1/AFBs have an additional, adenylate cyclase activity
255 with the responsible AC motif in the unannotated C-terminal region (Fig. 1, Fig. 2 and
256 Extended Data Fig. 3). As shown in Arabidopsis and moss, presumably, all TIR1/AFBs across
257 land plants have this activity. The N-terminal localized F-box and C-terminal AC motif are
258 spatially separated, suggesting that the ubiquitin ligase and AC activities are independent.

259 Hence, TIR1/AFBs represent a unique type of hormone receptor combining F-box and AC
260 motifs.

261 Auxin binding and AC activity sites are in spatial proximity within the TIR1 protein
262 structure (Extended Data Fig. 4a). Docking of ATP to TIR1 structure shows that V84 from the
263 Aux/IAA degron works like a latch to constrain the space available to ATP, suggesting it may
264 reduce its mobility and thus enhance the AC reaction efficiency (Fig. 3a). Indeed, auxin
265 together with the Aux/IAA co-receptors enhances the AC activity *in vitro* (Fig. 3b and
266 Extended Data Fig. 5). Moreover, cAMP content in roots starts to increase after auxin treatment
267 (Fig. 3c), and such increase is completely dependent on TIR1/AFBs auxin receptors (Fig. 3d).
268 Thus, auxin-activated cAMP production, in addition to Aux/IAA degradation, represents a
269 previously unsuspected signalling output from the TIR1/AFB-Aux/IAA co-receptor complex.
270 This implies the product of the AC activity - cAMP - as a second messenger in auxin signalling.

271 Accumulating evidence points to the existence of an elusive non-transcriptional branch of
272 TIR1/AFB auxin signalling mediating rapid cellular processes such as cytosolic Ca²⁺ spikes,
273 membrane depolarization and apoplast alkalinization^{13,14,16}, all linked to root growth inhibition¹².
274 Our expectation was that the newly identified AC activity of TIR1/AFBs would mediate these
275 rapid effects. Nonetheless, despite abolishing AC activity in TIR1^{ACm} variants renders them
276 incapable of mediating auxin-induced root growth inhibition (Fig. 4a-d), this effect does not
277 extend to the very rapid responses (Extended Data Fig. 7a,b). The *ccvTIR1^{ACm1}*-based root
278 growth resistance to *cvxIAA* (Extended Data Fig. 6a,b) as well as TIR1/AFB-mediated cAMP
279 production (Fig. 3c) have dynamics slower than 1 hour. Furthermore, mutating TIR1 AC
280 activity also compromises auxin-induced transcription of selected genes (Fig. 4f-j). These
281 observations suggest that AC activity of TIR1/AFB receptors contributes to the canonical,
282 transcriptional pathway and an additional mechanism is required for a very rapid response.

283 Historically, cNMPs are highly important and well established second messengers in
284 mammalian models²⁸. Comparably, cNMP research in plants is progressing slowly^{17,29}.
285 Nonetheless, the list of proteins with detected AC activity *in vitro* has been steadily
286 growing^{17,18,20-23} as for proteins with GC activity, which includes such prominent candidates as
287 the brassinosteroid and phytosulfokines receptors^{18,30,31}. Generally, the characterized plant
288 ACs/GCs have lower activities than their animal counterparts, and accordingly average cNMP
289 levels in plant tissues are also lower^{17,23}. Therefore, *in planta* relevance of the AC and GC
290 activities remains unclear and controversial, also due to the lack of genetic support and clearly
291 defined downstream effectors. Thus, the AC activity of TIR1/AFB auxin receptors and its key
292 importance for root growth regulation brings new prominence to the role of ACs in plants and
293 an incentive to rejuvenate cNMP signalling research in plant biology.

294

295 **References**

- 296 1 Friml, J. Fourteen stations of auxin. *Cold Spring Harb. Perspect. Biol.* **14**, a039859 (2021).
- 297 2 Parry, G. & Estelle, M. Auxin receptors: a new role for F-box proteins. *Curr. Opin. Cell*
298 *Biol.* **18**, 152-156 (2006).
- 299 3 Quint, M. & Gray, W. M. Auxin signaling. *Curr. Opin. Plant Biol.* **9**, 448-453 (2006).
- 300 4 Gray, W. M. et al. Identification of an SCF ubiquitin-ligase complex required for auxin
301 response in *Arabidopsis thaliana*. *Genes Dev.* **13**, 1678-1691 (1999).
- 302 5 Gray, W. M., Kepinski, S., Rouse, D., Leyser, O. & Estelle, M. Auxin regulates SCF^{TIR1}-
303 dependent degradation of AUX/IAA proteins. *Nature* **414**, 271-276 (2001).
- 304 6 Dharmasiri, N., Dharmasiri, S. & Estelle, M. The F-box protein TIR1 is an auxin receptor.
305 *Nature* **435**, 441-445 (2005).
- 306 7 Kepinski, S. & Leyser, O. The *Arabidopsis* F-box protein TIR1 is an auxin receptor. *Nature*
307 **435**, 446-451 (2005).
- 308 8 Tan, X. et al. Mechanism of auxin perception by the TIR1 ubiquitin ligase. *Nature* **446**,
309 640-645 (2007).
- 310 9 Prigge, M. J. et al. Genetic analysis of the *Arabidopsis* TIR1/AFB auxin receptors reveals
311 both overlapping and specialized functions. *eLife* **9**, e54740 (2020).
- 312 10 Kubes, M. & Napier, R. Non-canonical auxin signalling: fast and curious. *J. Exp. Bot.* **70**,
313 2609-2614 (2019).
- 314 11 Gallei, M., Luschnig, C. & Friml, J. Auxin signalling in growth: Schrodinger's cat out of
315 the bag. *Curr. Opin. Plant Biol.* **53**, 43-49 (2020).

- 316 12 Fendrych, M. et al. Rapid and reversible root growth inhibition by TIR1 auxin signalling.
317 *Nat. Plants* **4**, 453-459 (2018).
- 318 13 Li L. et al. Cell surface and intracellular auxin signalling for H⁺ fluxes in root growth.
319 *Nature* **599**, 273-277 (2021).
- 320 14 Serre, N. B. C. et al. AFB1 controls rapid auxin signalling through membrane
321 depolarization in *Arabidopsis thaliana* root. *Nat. Plants* **7**, 1229-1238 (2021).
- 322 15 Shih, H. W., DePew, C. L., Miller, N. D. & Monshausen, G. B. The cyclic nucleotide-gated
323 channel CNGC14 regulates root gravitropism in *Arabidopsis thaliana*. *Curr. Biol.* **25**, 3119-
324 3125 (2015).
- 325 16 Dindas, J. et al. AUX1-mediated root hair auxin influx governs SCF^{TIR1/AFB}-type Ca²⁺
326 signaling. *Nat. Commun.* **9**, 1174 (2018).
- 327 17 Gehring, C. Adenyl cyclases and cAMP in plant signaling - past and present. *Cell Commun.*
328 *Signal.* **8**, 15 (2010).
- 329 18 Wong, A., Gehring, C. & Irving, H. R. Conserved functional motifs and homology
330 modeling to predict hidden moonlighting functional sites. *Front. Bioeng. Biotechnol.* **3**, 82
331 (2015).
- 332 19 Swiezawska, B. et al. Molecular cloning and characterization of a novel adenylyl cyclase
333 gene, HpAC1, involved in stress signaling in *Hippeastrum x hybridum*. *Plant Physiol.*
334 *Biochem.* **80**, 41-52 (2014).
- 335 20 Al-Younis, I., Wong, A. & Gehring, C. The *Arabidopsis thaliana* K(+)-uptake permease 7
336 (AtKUP7) contains a functional cytosolic adenylate cyclase catalytic centre. *FEBS Lett.*
337 **589**, 3848-3852 (2015).

- 338 21 Al-Younis, I. et al. The Arabidopsis thaliana K(+)-uptake permease 5 (AtKUP5) contains
339 a functional cytosolic adenylate cyclase essential for K(+) transport. *Front. Plant Sci.* **9**,
340 1645 (2018).
- 341 22 Chatukuta, P. et al. An Arabidopsis clathrin assembly protein with a predicted role in plant
342 defense can function as an adenylate cyclase. *Biomolecules* **8**, 15 (2018).
- 343 23 Bianchet, C. et al. An Arabidopsis thaliana leucine-rich repeat protein harbors an adenylyl
344 cyclase catalytic center and affects responses to pathogens. *J. Plant Physiol.* **232**, 12-22
345 (2019).
- 346 24 Johnstone, T. B., Agarwal, S. R., Harvey, R. D. & Ostrom, R. S. cAMP signaling
347 compartmentation: adenylyl cyclases as anchors of dynamic signaling complexes. *Mol.*
348 *Pharmacol.* **93**, 270-276 (2018).
- 349 25 Parry, G. et al. Complex regulation of the TIR1/AFB family of auxin receptors. *PNAS* **106**,
350 22540-22545 (2009).
- 351 26 Uchida, N. et al. Chemical hijacking of auxin signaling with an engineered auxin-TIR1
352 pair. *Nat. Chem. Biol.* **14**, 299-305 (2018).
- 353 27 Li, L., Gallei, M. & Friml, J. Bending to auxin: fast acid growth for tropisms. *Trends Plant*
354 *Sci.* **27**, 440-449 (2022).
- 355 28 Beavo, J. A. & Brunton, L. L. Cyclic nucleotide research -- still expanding after half a
356 century. *Nat. Rev. Mol. Cell Biol.* **3**, 710-718 (2002).
- 357 29 Trewavas, A. J. Plant cyclic AMP comes in from the cold. *Nature* **390**, 657-658 (1997).
- 358 30 Kwezi, L. et al. The phytosulfokine (PSK) receptor is capable of guanylate cyclase activity
359 and enabling cyclic GMP-dependent signaling in plants. *J. Biol. Chem.* **286**, 22580-22588
360 (2011).

361 31 Wheeler, J. I. et al. The brassinosteroid receptor BRI1 can generate cGMP enabling cGMP-
362 dependent downstream signaling. *Plant J.* **91**, 590-600 (2017).

363

364 **Figure legends**

365 **Figure 1. TIR1/AFB auxin receptors have adenylate cyclase activity**

366 **a**, Alignment of the C-terminal protein sequences of TIR1/AFBs with the conserved AC motif.
367 LRR, leucine-rich repeat. The residues m1-m3 indicate the conserved key amino acids, which
368 were mutated to alanine to disrupt the AC activity (shown in Fig. 2).

369 **b-d**, *in vitro* AC activity of GST-AFB5 purified from *E.coli*. AC activity assay in the presence
370 of 2 different co-factors, followed by cAMP quantification by EIA (Enzyme ImmunoAssay)
371 kit. The values shown were blanked against the background signals from the corresponding
372 GST samples (**b**). Typical LC-MS/MS spectrum showing cAMP detection in the AC reaction
373 with the characteristic peak used for quantification (**c**). Michaelis-Menten kinetics for the AC
374 activity quantified by LC-MS/MS. S, substrate; V, velocity (**d**). For each data point, means \pm
375 SD from 3 biological replicates are shown.

376 **e**, *in vitro* AC activity of His-GFP-FLAG-TIR1 purified from *Sf9* insect cells. Michaelis-
377 Menten kinetics giving results similar to GST-AFB5 (shown in d).

378

379 **Figure 2. C-terminal AC motif is responsible for the TIR1/AFB AC activity**

380 **a-b**, C-terminal AC motif is essential for the AFB5 AC activity. The AC deficient *E. coli* strain
381 SP850 was complemented by the indicated constructs. The red colour of the MacConkey agar
382 indicates the presence of AC activity. The empty vector *pGEX-4T-1* was used as negative
383 control. Western blot confirms similar expression levels of endogenous and mutated AFB5
384 proteins. Ponceau staining of the membrane was used as the loading control (**a**). *in vitro* AC
385 activity assay for the purified GST-AFB5 and 3 mutated variants, followed by the cAMP

386 quantification using LC-MS/MS. V, velocity. The values shown are means \pm SD from 3
387 biological replicates (**b**).

388 **c**, C-terminal AC motif is essential for the AC activity of TIR1 ^{Δ NT}. GST-TIR1 ^{Δ NT} and 3
389 mutated variants were purified from *E. coli*. An *in vitro* AC activity assay was performed
390 followed by cAMP quantification using LC-MS/MS. V, velocity. The values shown are means
391 \pm SD from 3 biological replicates.

392 **d**, Pull-down results showing differential effects of TIR1^{ACm} mutations on the IAA-induced
393 TIR1-Aux/IAA interaction. Wild-type and the 3 mutated TIR1 variants were translated *in vitro*
394 using wheat germ extracts, and were then used for pull-down assays with purified GST-IAA7,
395 in the presence or absence of 10 μ M IAA as indicated.

396

397 **Figure 3. Auxin perception enhances the TIR1/AFBs AC activity**

398 **a**, Docking of ATP on the surface of TIR1-IAA-Aux/IAA complex. The beginning of the AC
399 center was labelled in magenta. Amino acids presumably important for the AC activity were
400 labelled either in red (acidic), or in blue (basic). E554 is the site for m1 (as in Fig. 1a). Note
401 that V84 from the Aux/IAA degron restricts the space available to ATP.

402 **b**, Auxin together with Aux/IAA stimulates the TIR1 AC activity. *in vitro* AC activity assay
403 with His-GFP-FLAG-TIR1 (5 μ g) in the presence of 10 μ M IAA, IAA7 (3 μ g), IAA17 (3 μ g)
404 and the indicated combinations, followed by cAMP quantification using LC-MS/MS. V,
405 velocity. One-way ANOVA. n = 3. *** $p \leq 0.001$; **** $p \leq 0.0001$.

406 **c**, Auxin treatment increases cAMP content in root tissues. Five-days-old Col-0 seedlings were
407 treated with 100 nM IAA. Root tissues were harvested for cAMP quantification by LC-MS/MS.
408 One-way ANOVA. n = 3. * $p \leq 0.05$.

409 **d**, Auxin-induced increase of cAMP levels in roots is dependent on TIR1/AFBs. Five-days-old
410 Col-0 or *tir* triple seedlings were treated with 100 nM IAA for 6 h. Root tissues were collected
411 for cAMP measurement by LC-MS/MS. One-way ANOVA. $n = 3$. * $p \leq 0.05$. ns, not
412 significant.

413

414 **Figure 4. TIR1 AC activity contributes to auxin-induced root growth inhibition and**
415 **transcriptional responses**

416 **a-b**, AC motif mutations compromise TIR1 function in mediating IAA-induced root growth
417 inhibition. *pTIR1::TIR1* and the similar constructs containing the 3 AC motif mutations were
418 transformed into *tir1-1 afb2-3*. Representative examples of 6-days-old seedlings of different
419 genotypes grown on Mock or 100 nM IAA containing medium. Bar = 10 mm (**a**).
420 Quantification of the root length in (a). $n = 30$ (**b**).

421 **c**, Simplified scheme showing the principles of the engineered cvxIAA/ccvTIR1 system.

422 **d**, C-terminal AC motif is crucial for cvxIAA-triggered root growth inhibition in *ccvTIR1* line.
423 *pTIR1::TIR1*, *pTIR1::ccvTIR1*, and the 3 similar constructs containing the AC motif mutations
424 (see Fig. 1a) were transformed into *tir1-1 afb2-3*. Root length of the 6-days-old seedlings with
425 different genotypes grown on Mock or 500 nM cvxIAA containing medium were measured. n
426 = 30.

427 **e**, AC activity is required for TIR1 function in root gravitropism. Five-days-old seedlings of
428 the indicated genotypes were transferred to new plates. The plates were rotated 90 degree
429 before images were captured every 30 min. Root bending angle was measured to monitor the
430 gravitropic response. $n = 10$.

431 **f-j**, AC activity contributes to auxin-induced genes expression. Five-days-old seedlings were
432 either Mock-treated or treated with liquid medium containing 200 nM cvxIAA for 3 h.
433 Seedlings were harvested for RNA extraction and qRT-PCR. Shown are the relative expression
434 values normalized to the internal control *PP2AA3*, from 3 or 4 biological replicates.

435

436 **Methods**

437 **Plant materials and growth conditions**

438 All the *Arabidopsis* mutants and transgenic lines used in this study are in Columbia-0 (Col-0)
439 background. The *tir1-1 afb2-3* mutant was shared by Keiko U. Torii²⁶. The *tir1-1 afb2-1 afb3-*
440 *I*³², and the calcium sensor GCaMP3³³ have been described previously. To generate the
441 complementation lines *pTIR1::TIR1*, *pTIR1::TIR1^{ACm1}*, *pTIR1::TIR1^{ACm2}* and
442 *pTIR1::TIR1^{ACm3}* in *tir1-1 afb2-3*, *TIR1* promoter sequence was amplified from genomic DNA
443 and cloned into pDONR P4-P1r, and the *TIR1* CDS (coding domain sequence) was cloned into
444 pDONR221. To mutate the AC motif in *TIR1*, Phusion Site-Directed Mutagenesis Kit (Thermo
445 Fisher, F541) was used, with the plasmid of *TIR1* in pDONR221 as the template. The resulting
446 entry clones were recombined into the destination vector pB7m24GW to get the final
447 expression vectors. The constructs *pTIR1::ccvTIR1* and the mutated versions
448 *pTIR1::ccvTIR1^{ACm1}*, *pTIR1::ccvTIR1^{ACm2}* and *pTIR1::ccvTIR1^{ACm3}* were generated in a similar
449 way. F79G mutation was used to generate the engineered ccvTIR1 according to the previous
450 report²⁶. All the primers used for plasmid construction are listed in Extended Data Table 1. The
451 final expression constructs were transformed into the *Agrobacterium tumefaciens* strain
452 GV3101 by electroporation. Floral dip method was used to transform the *Arabidopsis* plants.

453 Seeds were surface-sterilized by chlorine gas, sown on half-strength Murashige and Skoog
454 ($\frac{1}{2}$ MS) medium supplemented with 1% (w/v) sucrose and 0.8% (w/v) phyto agar (pH 5.9),
455 stratified in the dark at 4°C for 2 days and then grown vertically at 21°C with a long-day
456 photoperiod (16 h light/8 h dark). Light sources used were Philips GreenPower LED production
457 modules [in deep red (660 nm)/far red (720 nm)/blue (455 nm) combination, Philips], with a
458 photon density of 140.4 $\mu\text{mol}/\text{m}^2/\text{s} \pm 3\%$ ¹³.

459

460 **Root growth assays**

461 Seeds were directly sown on plates containing different treatment medium. Six-days-old
462 seedlings were scanned with a horizontal scanner (Epson Perfection V800 Photo) to acquire
463 images. Root length was measured using the segmentation plugin Simple Neurite Tracer in
464 Image J³⁴. To track the root growth dynamics, a vertical scanner growth assay was performed
465 as previously described¹³. Simply, five-days-old seedlings were transferred to petri dishes filled
466 with treatment medium. The petri dishes were fixed with a mold into a vertically mounted
467 scanner (Epson Perfection v.370), so that root can grow vertically during imaging. Roots were
468 imaged automatically every 30 min using the AutoIT script described previously³⁵. The
469 resulting image series were registered using StackReg and root growth rate was measured using
470 the Manual Tracking plugin in ImageJ. To evaluate root growth in a high temporal resolution,
471 the microfluidic vRootchip was used as previously described^{12,13}. For root gravitropism assay,
472 it was done in a similar way with the vertical scanner growth assay, except the plates with
473 seedlings were rotated 90 degree to give a gravi-stimulation when placed onto the vertical
474 scanner. Root bending angles were measured based on the output from the Manual Tracking
475 plugin in ImageJ.

476

477 ***E. coli* complementation assay**

478 The *E. coli* SP850 strain (lam-, el4-, relA1, spoT1, cyaA1400(:kan), thi-1), deficient in
479 adenylate cyclase, was originally obtained from the *E. coli* Genetic Stock Center (Yale
480 University, New Haven, USA) (accession number 7200) and shared by Krzysztof Jaworski.
481 The positive control HpAC1¹⁹, and the potential candidate genes TIR1/AFBs were cloned into
482 pGEX-4T-1. The primers and restriction sites used are listed in Extended Data Table 1. The
483 overnight SP850 cultures (10 μ L) containing the indicated constructs were streaked onto

484 MacConkey agar with ampicillin (100 µg/ml) and IPTG (100 µM). The plates were incubated
485 at 37°C for 12 h, and the images were obtained.

486

487 **Western blot**

488 The overnight SP850 cultures containing different constructs were inoculated at the dilution of
489 1:100 into LB medium with ampicillin (100 µg/ml) and IPTG (100 µM), and were then cultured
490 at 37°C for another 6 h for protein induction. Cells were pelleted from equal volume of the
491 induced cultures (1 mL), directly lysed in Laemmli Sample Buffer (Biorad, 1610747), and
492 denatured at 95°C for 5 min. Supernatants were loaded into 10% precast gel (Mini-Protean®
493 TGX™, Bio-Rad). After separation, proteins were transferred to PVDF membranes by
494 electroblotting (Trans-blot® Turbo™, Bio-Rad). The immunoblotting was performed
495 following the standard procedure with the anti-GST-tag, HRP-conjugated monoclonal antibody
496 (Agrisera, AS18 4188) at the dilution of 1:2000. Chemiluminescence signal was detected with
497 Bio-Rad ChemiDoc™ MP Imager. Ponceau staining of the membrane was used to show the
498 equal loading.

499

500 **Protein purification**

501 Gene sequences for protein expression in *E. coli* were cloned into pGEX-4T-1 vector using the
502 primers listed in Extended Data Table 1. The resulting plasmids were introduced into the BL21
503 competent cells (NEB, C2530H) in order to produce the fusion proteins with GST (glutathione-
504 S-transferase) affinity tag. The transformants were grown in LB medium (500 mL) containing
505 ampicillin (100 µg/mL) and 2% glucose at 37°C. Fusion protein expression was induced by
506 adding IPTG (isopropyl-β-D-thiogalactopyranoside) to a final concentration of 0.5 mM at
507 OD₆₀₀ = 0.6 and incubating the culture at 18°C for 4 h. The bacteria were harvested by

508 centrifugation and the pellet was suspended in lysis buffer (50 mM Tris-HCl pH 8.0, 150 mM
509 NaCl, 5 mM EDTA, 5 mM EGTA, 1% (v/v) Triton X-100, 1 mM PMSF, 0.2 mg/mL lysozyme)
510 and disrupted by sonication. The cell extract was centrifuged at $18,000 \times g$ for 35 min and the
511 supernatant was loaded onto a glutathione-Sepharose 4B beads (GE Healthcare). Afterward,
512 the column was washed multiple times with buffer containing 50 mM Tris-HCl (pH 8.0), 150
513 mM NaCl and the GST fusion protein was eluted with 10 mM glutathione in 50 mM Tris-HCl
514 (pH 9.0). The homogeneity and purity of eluted protein fraction was analyzed by SDS-PAGE
515 electrophoresis (8% gel) with the Coomassie Blue gel staining.

516 To remove GST affinity tag by thrombin cleavage, the cell extract after centrifugation at
517 $18,000 \times g$ for 35 min was loaded onto a GStap™ FF column using an ÄKTA start system
518 (GE Healthcare). After washing the column with binding buffer (140 mM NaCl, 2.7 mM KCl,
519 10 mM Na₂HPO₄, 1.8 mM KH₂PO₄, pH 7.3), 20 U of thrombin (Sigma, 604980) was dissolved
520 in binding buffer and applied to the column via 1 mL loop. The column was sealed and
521 incubated at 22°C for 6 h. After incubation, the HiTrap™ Benzamidine FF column (Sigma,
522 GE17-5143-02) was placed in series directly after the GStap™ FF column for thrombin
523 binding. The columns were washed with binding buffer and the pure proteins were collected in
524 0.5 mL fractions. The homogeneity and purity of eluted protein fraction was analyzed by SDS-
525 PAGE electrophoresis (8% gel) with the Coomassie Blue gel staining.

526 To purify TIR1 full-length protein from *Sf9* insect cells. A vector was constructed to co-
527 express His-GFP-(TEV)-FLAG-TIR1 and His-(TEV)-ASK1. Generation of recombinant virus
528 and infection were all done as previously described^{36,37}. To purify TIR1 protein, the frozen cell
529 pellets were thawed and resuspended in lysis buffer containing equal volumes of CytoBuster™
530 Protein Extraction Reagent (Millipore, 71009-3) and buffer A (20 mM Tris-HCl pH 7.4, 200
531 mM NaCl, 1 mM EDTA, Protease Inhibitor Cocktail (Sigma) and 1 mM TCEP). The lysis
532 solution was mixed by rolling at 4°C for 45 min. Lysate was then disrupted by sonication and

533 centrifuged at $20,000 \times g$ for 20 min. The supernatant was collected and filtered through a 0.45
534 μm and 0.2 μm filters (Merck). All subsequent steps took place in the cold room at 4°C . Before
535 applying the sample to the nickel metal affinity chromatography column, cOmplete His-Tag
536 Purification Resin (Roche) was washed and equilibrated with buffer A for 1 h. Filtrate was then
537 loaded onto the conditioned column and the resin was washed with 5 volumes of buffer A.
538 Then the resin was washed with 5 volumes of buffer A (without TCEP) containing 10 mM
539 imidazole. Fusion protein was eluted with buffer B (buffer A, 250 mM imidazole). Eluted
540 proteins were then loaded onto Pierce™ Anti-FLAG Affinity Resin (Thermo Scientific,
541 A36801), previously equilibrated with buffer A, to remove free ASK1 protein. The column
542 was placed on a rotor and mixed for 1 h. Resin was then washed 3x with 5 bed volumes of PBS
543 (pH 7.2) and 1x with 5 bed volumes of purified water. Fusion TIR1 protein was eluted with 2
544 mL of 1.5 mg/mL Pierce™ 3x DYKDDDDK peptide (Thermo Scientific, A36805), according
545 to manufacturer instructions. FLAG peptide was then removed by desalting using Zeba™ Spin
546 Desalting Columns (Thermo Scientific, 89891), according to manufacturer instructions. The
547 homogeneity and purity of protein was analyzed by SDS-PAGE electrophoresis (8% gel) with
548 the Coomassie Blue gel staining.

549

550 ***in vitro* AC activity assay**

551 *in vitro* AC activity of the purified proteins was determined by evaluating the rate of cAMP
552 formation. The reaction mixture contained: 10 mM Tris-HCl buffer (pH 7.6), 1 mM MgCl_2
553 and/or 1 mM MnCl_2 , 1 mM IBMX (3-isobutyl-1-methylxanthine), 1 mM ATP, 1 mM DTT and
554 5 μg of the protein in a final volume of 100 μL . To investigate the effects of IAA on the AC
555 activity of AFB5, 10 μM IAA was added to the reaction mixture along with 5 μg of IAA7 or
556 IAA17. Samples were then incubated at 30°C for 25 min. The enzyme reaction was terminated

557 by incubation at 100 °C for 10 min and the samples were centrifuged at 16,100 × g for 10 min.
558 The cAMP level after the reaction was quantified using either the Amersham cAMP Biotrak
559 Enzymeimmunoassay system (GE, RPN225) or LC-MS/MS. For cAMP measurement with
560 enzyme immunoassay, the acetylation assay was performed following the standard procedures
561 of Protocol 2 in the product booklet. The AC reaction product was diluted 10 fold with assay
562 buffer during the assay.

563

564 **Root cAMP extraction and quantification**

565 Five-days-old Col-0 or *tir* triple seedlings grown in 12 cm × 12 cm square plates were sprayed
566 with 20 mL of ½ MS liquid medium without or with 100 nM IAA per plate. At the indicated
567 time points, root tissues were harvested and immediately frozen in liquid nitrogen. Isolation of
568 cAMP from root tissues was carried out according to the published method³⁸, with minor
569 changes. Frozen roots were homogenized manually with a pre-cooled mortar and pestle with
570 liquid nitrogen. The grounded powder was weighed and about 100 mg of sample was
571 transferred to a 2 mL Eppendorf tube and 600 µL of 4% acetic acid together with 10 µL of
572 IBMX (1 mM) were added. Sample was vortexed for 30 s and centrifuged for 5 min at 5000 ×
573 g at 4 °C. The supernatant was collected, 1200 µL of acetonitrile was added and the sample
574 was centrifuged again for 5 min at 5000 × g at 4°C. The supernatant was transferred to a 15
575 mL Falcon® tube and 200 µL of 5/95 100 mM ammonium formate/acetonitrile buffer, 200 µL
576 of water and 2 mL of acetonitrile were added. Subsequently the sample was vortexed for 1 min
577 and centrifuged for 5 min at 2000 × g. The supernatant was then transferred to the silica
578 Discovery® DSC-18 SPE 1 mL Tube (Sigma, St. Louis MO, USA), that was first conditioned
579 with 2.5 mL of water under vacuum conditions and equilibrated with 2.5 mL of 5/95 100 mM
580 ammonium formate/acetonitrile. The supernatant was slowly drawn through the SPE cartridge

581 by vacuum conditions. After sample loading the SPE tube was washed with 1 mL of 10/90
582 water/acetonitrile and the analyte was eluted with 0.5 mL of water followed by filtering (0.2
583 μm , Merck, Ireland). The samples were lyophilized, reconstituted in 50 μL of water and 5 μL
584 was injected into the LC–MS/MS system for analysis.

585

586 **LC-MS/MS (Liquid chromatography-tandem mass spectrometry) analysis**

587 LC-MS/MS experiments were performed using the Nexera UHPLC and LCMS-8045
588 integrated system (Shimadzu Corporation). The ionization source parameters were optimized
589 in positive ESI mode using pure cAMP dissolved in HPLC-grade water (Sigma). Samples were
590 separated at 40°C using a XSelect CSH Phenyl-Hexyl column (100 x 2.1 mm, 3.5 μm , Waters).
591 An isocratic flow of 90% solvent A (0.05% (v/v) formic acid with 5 mM ammonium formate)
592 and 10% solvent B (100% (v/v) acetonitrile) was applied over 5 min, followed by washing and
593 conditioning of the column, with a flow rate of 0.4 mL/min. The interface voltage was set at
594 4.0 kV for positive (ES+) electrospray. Data acquisition and analysis were made with the
595 LabSolutions workstation for LCMS-8045.

596

597 **Pull-down assays**

598 The coding sequence of TIR1-HA was cloned into pF3A WG (BYDV) Flexi® Vector
599 (Promega, L5671) for *in vitro* translation. Similar TIR1^{ACms}-HA constructs were obtained using
600 Phusion Site-Directed Mutagenesis Kit (Thermo Fisher, F541). 3 μg of plasmids were used for
601 each 50 μL of *in vitro* translation reaction using TnT® SP6 High-Yield Wheat Germ Protein
602 Expression System (Promega, L3260). For pull-down, 20 μL of *in vitro* translated proteins
603 were incubated with 5 μg of GST-IAA7 purified from *E. coli*, in the presence or absence of 10
604 μM IAA at 4°C for 1 h. The incubation buffer used is 50 mM Tris-HCl (pH 7.5), 100 mM

605 NaCl, 10% glycerol, 10 μ M MG132 and complete mini-protease inhibitors cocktail (Roche).
606 Then 40 μ L of Glutathione agarose (Thermo Scientific, 16102) was equilibrated, added into
607 the reaction, and incubated for another 1 h at 4°C. Glutathione beads were recovered by a brief
608 centrifugation and washed three times with 1 mL of washing buffer (50 mM Tris-HCl (pH 7.5),
609 100 mM NaCl, 10% glycerol, 0.1% Tween 20) containing the same amount of IAA as the
610 incubation buffer. Western blot was performed as described above using Anti-HA-Peroxidase
611 (Sigma, 12013819001) and anti-GST-tag, HRP-conjugated monoclonal antibody (Agrisera,
612 AS18 4188).

613

614 **Molecular docking**

615 To carry out the molecular docking of ATP on TIR1, the published crystal structure available
616 under PDB code 2P1Q was used⁸. Then crystallographic waters as well as the co-crystallized
617 ASK1 adaptor protein were removed, and by using AutoDockTools³⁹ polar hydrogens were
618 added to the structure and the file was converted to pdbqt format. Avogadro²⁴⁰ and
619 OpenBabel⁴¹ were used to draw the molecule of ATP, perform an initial geometry optimization,
620 and protonate it for a pH of 7.4. Subsequently, a pdbqt file was created for ATP using
621 AutoDockTools. Docking was performed using AutoDock Vina⁴², which allows one to obtain
622 results with high accuracy whilst retaining substantial speed. Because of the many degrees of
623 freedom of the ATP molecule, a very high search exhaustiveness was used, to ensure that the
624 whole conformational space was adequately sampled. Visualizations were created using UCSF
625 Chimera⁴³. Molecular surfaces were generated via MSMS⁴⁴, and the rendering was performed
626 with PoV-Ray.

627

628 **Microfluidic vRootchip and live imaging**

629 The microfluidic vRootchip coupled to an in-house-established vertical Zeiss LSM 800
630 confocal microscope was used to analyze the rapid root growth inhibition, and monitor
631 cytosolic Ca²⁺ level and apoplastic pH in real time, according to the previously established
632 procedures in the lab^{12,13}. The reported calcium sensor GCaMP3³³ was crossed with the different
633 homozygous transgenic lines generated in this study, and the F1 seedlings were directly used
634 for imaging analysis. GFP (excitation, 488 nm; emission, 514 nm) signal in the epidermal cells
635 of root elongation zone was captured every 15 s with a Plan-Apochromat ×20/0.8 NA air
636 objective, and was then quantified using Image J. To measure apoplastic pH lively, a
637 ratiometric fluorescent pH dye HPTS was added into the vRootchip medium at a final
638 concentration of 1 mM. Fluorescence signals for protonated HPTS (excitation, 405 nm;
639 emission, 514 nm) and deprotonated HPTS (excitation, 488 nm; emission, 514 nm) were
640 detected with the same ×20/0.8 NA air objective. Image analysis was performed using batch
641 processing of a previously described ImageJ macro⁴⁵.

642

643 **Quantitative real-time PCR (qRT-PCR)**

644 Five-days-old seedlings were transferred to ½ MS liquid medium (Mock) or medium
645 containing 200 nM cvxIAA. Each treatment has 3 or 4 biological replicates. Seedlings were
646 harvested at 3 h after treatment for RNA extraction with RNeasy Plant Mini Kit (QIAGEN,
647 74904). 1 µg of total RNA was used for reverse transcription after removal of genomic DNA
648 according to the instructions of RevertAid First Strand cDNA Synthesis Kit (Thermo, K1622).
649 cDNA was diluted 20 fold before qRT-PCR. Samples were pipetted in 3 technical replicates
650 using an Automated Workstation Biomek i5 (Beckman Coulter). qRT-PCR was performed
651 with LightCycler 480 (Roche) using Luna Universal qPCR Master Mix (NEB, M3003S).
652 Sequences of the gene-specific primers used are all listed in Extended Data Table 1, and most

653 of them are actually directly taken from the previous publication²⁶. Relative gene expression
654 level was calculated using $\Delta\Delta$ CT method with Protein Phosphatase 2A Subunit A3 (PP2AA3)
655 as the internal control.

656

657 **Software and statistical analysis**

658 Multiple sequence alignment was performed using the software Jalview⁴⁶. The TIR1 3D
659 structure (2p1q) was visualized and labelled in PDBe (Protein Data Bank in Europe). All graphs
660 were generated using GraphPad Prism 8. One-way ANOVA, two-way ANOVA and multiple
661 comparisons were performed where necessary using GraphPad Prism 8.

662

663 **Methods references**

- 664 32 Dharmasiri, N. et al. Plant development is regulated by a family of auxin receptor F box
665 proteins. *Dev. Cell* **9**, 109-119 (2005).
- 666 33 Toyota, M. et al. Glutamate triggers long-distance, calcium-based plant defense signaling.
667 *Science* **361**, 1112-1115 (2018).
- 668 34 Longair, M. H., Baker, D. A. & Armstrong, J. D. Simple Neurite Tracer: open source
669 software for reconstruction, visualization and analysis of neuronal processes.
670 *Bioinformatics* **27**, 2453-2454 (2011).
- 671 35 Li, L., Krens, S. F. G., Fendrych, M. & Friml, J. Real-time analysis of auxin response, cell
672 wall pH and elongation in *Arabidopsis thaliana* hypocotyls. *Bio. Protoc.* **8**, e2685 (2018).
- 673 36 Lee, S. et al. Defining binding efficiency and specificity of auxins for SCF^{TIR1/AFB}-Aux/IAA
674 co-receptor complex formation. *ACS Chem. Biol.* **9**, 673-682 (2014).
- 675 37 Quareshy, M. et al. The tetrazole analogue of the auxin indole-3-acetic acid binds
676 preferentially to TIR1 and not AFB5. *ACS Chem. Biol.* **13**, 2585-2594 (2018).
- 677 38 Van Damme, T. et al. Wounding stress causes rapid increase in concentration of the
678 naturally occurring 2',3'-isomers of cyclic guanosine- and cyclic adenosine monophosphate
679 (cGMP and cAMP) in plant tissues. *Phytochemistry* **103**, 59-66 (2014).
- 680 39 Morris, G. M. et al. AutoDock4 and AutoDockTools4: Automated docking with selective
681 receptor flexibility. *J. Comput. Chem.* **30**, 2785-2791 (2009).
- 682 40 Hanwell, M. D. et al. Avogadro: an advanced semantic chemical editor, visualization, and
683 analysis platform. *J. Cheminform.* **4**, 17 (2012).
- 684 41 O'Boyle, N. M. et al. Open Babel: An open chemical toolbox. *J. Cheminform.* **3**, 33 (2011).

685 42 Trott, O. & Olson, A. J. AutoDock Vina: improving the speed and accuracy of docking
686 with a new scoring function, efficient optimization, and multithreading. *J. Comput. Chem.*
687 **31**, 455-461 (2010).

688 43 Pettersen, E. F. et al. UCSF Chimera--a visualization system for exploratory research and
689 analysis. *J. Comput. Chem.* **25**, 1605-1612 (2004).

690 44 Sanner, M. F., Olson, A. J. & Spehner, J. C. Reduced surface: an efficient way to compute
691 molecular surfaces. *Biopolymers* **38**, 305-320 (1996).

692 45 Barbez, E., Dunser, K., Gaidora, A., Lendl, T. & Busch, W. Auxin steers root cell
693 expansion via apoplastic pH regulation in *Arabidopsis thaliana*. PNAS 114, E4884-E4893
694 (2017).

695 46 Waterhouse, A. M., Procter, J. B., Martin, D. M., Clamp, M. & Barton, G. J. Jalview
696 Version 2--a multiple sequence alignment editor and analysis workbench. *Bioinformatics*
697 **25**, 1189-1191 (2009).

698
699

700 **Acknowledgements**

701 This research was supported by the Life Science Facility (LSF) and the Bioimaging Facility
702 (BIF) of IST Austria. We are grateful for the suggestions and advice from Chris Gehring, and
703 the seeds and plasmids shared from Keiko U. Torii and Gary Stacey. This project was funded
704 by the European Research Council Advanced Grant (ETAP-742985). M.F.K. and R.N.
705 acknowledge the support of EU MSCA-IF project CrysPINs (792329). M.K. was supported by
706 the project POWR.03.05.00 - 00 - Z302/17 Universitas Copernicana Thoruniensis in Futuro -
707 IDS “Academia Copernicana”. CIDG acknowledges support from UKRI under Future Leaders
708 Fellowship grant number MR/T020652/1.

709

710 **Author contributions**

711 L.Q. and J.F. conceived and designed the experiments. L.Q. carried out most of the
712 experiments. M.K. and K.J. performed most of the protein purification, *in vitro* AC activity
713 assay and LC-MS/MS analysis. H.C. performed the vRootchip experiments. L.H. assisted with
714 the root growth tracking with vertical microscope. M.Z. did the root gravitropism assay. S.S.
715 originally tested relationship between auxin and eATP signaling. M.F.K. and R.N. assisted
716 with TIR1 expression in insect cells. C.I.D.G. performed the molecular docking. L.Q. and J.F.
717 wrote the manuscript.

718

719 **Competing interests**

720 The authors declare there are no competing interests.

721

722 **Additional information and correspondence**

723 All the main data supporting the conclusion of this study are available in the paper and its

724 Extended Information. Additional data are available from the corresponding author upon

725 reasonable request. Correspondence and material request should be addressed to J.F.

726

727 **Extended Data Figure/Table Legends**

728 **Extended Data Figure 1. Additional data to support the AC activity of TIR1/AFBs**

729 **a-b**, *E. coli* complementation assay showing that AFB1 and AFB5 have AC activity. The AC
730 deficient SP850 strain was complemented with the empty vector (*pGEX-4T-1*), the positive
731 control (HpAC1), and TIR1/AFBs. Red colour of the MacConkey Agar indicates the presence
732 of AC activity (a). Western blot result shows that only AFB1 and AFB5 can be visibly detected
733 among the 6 members of TIR1/AFBs. Ponceau red staining of the membrane was used as the
734 loading control.

735 **c**, Michaelis-Menten kinetics for the AC activity of GST-AFB1 purified from *E. coli*. cAMP
736 level after reaction was quantified by LC-MS/MS. S, substrate; V, velocity. For each data point,
737 means \pm SD from 3 biological replicates are shown.

738 **d**, Representative LC-MS/MS spectrum showing the detection of cAMP after the *in vitro* AC
739 activity assay for His-GFP-FLAG-TIR1 purified from *Sf9* insect cells.

740

741 **Extended Data Figure 2. Gel images showing the purity of all the proteins used**

742 **a**, GST-AFB5. **b**, GST-AFB1. **c**, His-GFP-FLAG-TIR1. **d**, GST-PpAFB1. **e**, GST-PpAFB2. **f**,
743 GST-PpAFB3. **g**, GST-PpAFB4. **h**, GST-AFB5^{ACm1/m2/m3}. **i**, GST-TIR1 ^{Δ NT}. **j**, GST-TIR1 ^{Δ NT}-
744 ^{ACm1/m2/m3}. **k**, AFB5 after cleavage of GST tag. **l**, IAA7 after cleavage of GST tag. **m**, IAA17
745 after cleavage of GST tag. His-GFP-FLAG-TIR1 was purified from *Sf9* insect cells. All the
746 other proteins were purified from BL-21 *E. coli* cells. Proteins were separated on SDS-PAGE
747 gels and the gels were stained with Coomassie Brilliant Blue.

748

749 **Extended Data Figure 3. AC activity is conserved in TIR1/AFBs orthologues from**
750 ***Physcomitrella***

751 **a**, Alignment of the C-terminal protein sequences of TIR1/AFBs together with their
752 orthologues from *Physcomitrella*. Note the AC motif is highly conserved in all the sequences.
753 Only the first amino acid is a bit more relaxed.

754 **b**, TIR1/AFBs orthologues from *Physcomitrella* have AC activity. GST-tagged PpAFBs were
755 purified from *E. coli*. *in vitro* AC activity assay was performed with GST as the negative
756 control. cAMP level after reaction was quantified using LC-MS/MS. The values shown are
757 means \pm SD from 3 biological replicates. One-way ANOVA. ** $p \leq 0.01$; **** $p \leq 0.0001$.

758

759 **Extended Data Figure 4. Protein structure of TIR1-IAA-Aux/IAA complex and ribbon**
760 **structure showing ATP docking**

761 **a**, Protein structure of TIR1-IAA-Aux/IAA complex showing the spatial position of the C-
762 terminal AC motif. Different parts were labelled as different colours. Dark green, ASK1; Red,
763 TIR1; White, C-terminal AC motif; Blue, IAA7 peptide; Yellow, InsP₆ (inositol
764 hexakisphosphate); Green, IAA.

765 **b**, Ribbon structure showing the interaction of ATP with the key amino acids of the AC motif.
766 AC center was labelled in magenta. E554 is the residue identified for m1 in Fig. 1a, R566 for
767 m2, and D568 for m3. Note that V84 from the Aux/IAA degron restricts the space available to
768 ATP.

769

770 **Extended Data Figure 5. Auxin perception enhances the AC activity of AFB5**

771 *in vitro* AC activity assay for AFB5 in the presence of 10 μ M IAA, IAA7, IAA17 and the
772 indicated combinations, followed by cAMP quantification using LC-MS/MS. Tag-cleaved
773 clean proteins were used for this experiment. One-way ANOVA. n = 3. ** $p \leq 0.01$; **** $p \leq$
774 0.0001.

775

776 **Extended Data Figure 6. Delayed requirement of the AC activity in root growth**
777 **regulation**

778 **a**, Loss of AC activity does not affect cvxIAA/ccvTIR1-induced root growth inhibition within
779 the first hour. A vRootchip experiment was performed with the transgenic lines indicated, and
780 the images were captured with a time interval of 1 min. Mock medium was changed to medium
781 containing 500 nM of cvxIAA at 40 min. Root growth rate was normalized to the starting point
782 of the respective group. n = 4.

783 **b**, Resistance of ccvTIR1^{ACm1} to cvxIAA-triggered root growth inhibition occurs only after 1
784 h of treatment. Vertical scanner growth assay was performed to track the root growth dynamics.
785 Five-days-old seedlings of the indicated genotypes were transferred to either Mock medium or
786 medium containing 200 nM of cvxIAA. Images were taken every 30 min. Root growth rate
787 was measured. n = 10.

788

789 **Extended Data Figure 7. TIR1 AC activity is not crucial for rapid auxin responses**

790 **a**, cvxIAA triggers similar Ca²⁺ spikes in the *ccvTIR1* and *ccvTIR1*^{ACm1} lines. The calcium
791 sensor GCaMP3 was crossed to the indicated transgenic lines. Five-days-old F1 seedlings were
792 used for vRootchip experiment, and the images were captured with a time interval of 15 s.
793 Mock medium was changed to medium containing 500 nM of cvxIAA at 10 min. The

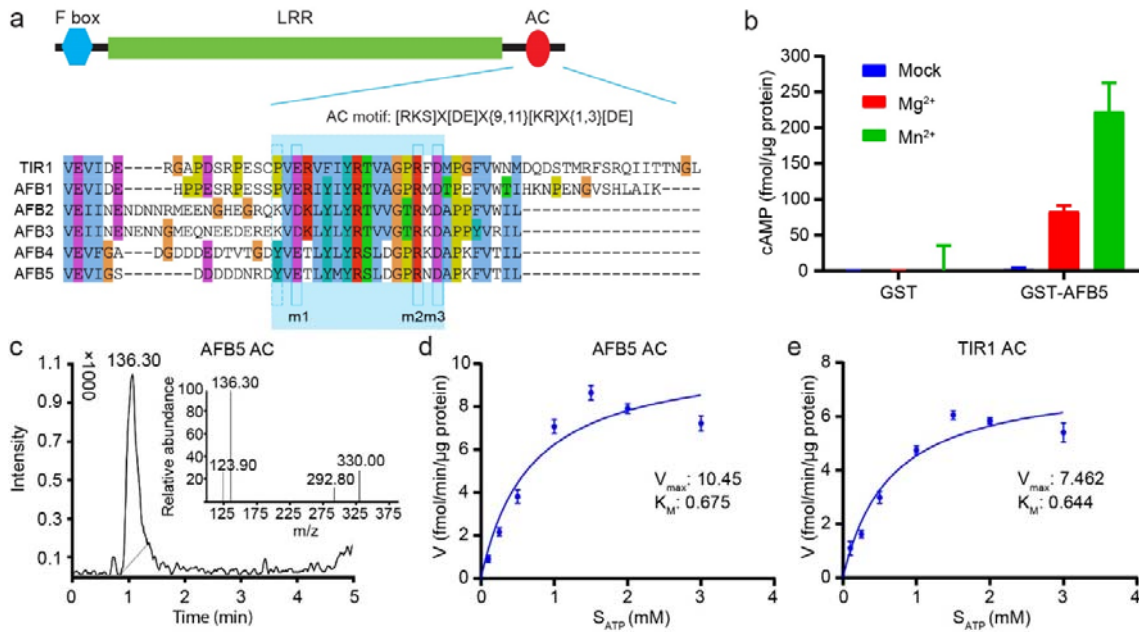
794 fluorescence signal in the epidermal cells of root elongation zone was quantified, and was
795 normalized to the average value of time points before treatment. n = 4.

796 **b**, Auxin-induced apoplastic alkalinisation is not changed in the *TIRI^{ACm1}* line. Five-days-old
797 seedlings of the indicated genotypes were used for vRootchip experiment. Mock medium was
798 changed to medium containing 10 nM of IAA at 11 min. Ratiometric (488 nm/405nm) imaging
799 of HPST staining was used to measure apoplastic pH in the epidermal cells of root elongation
800 zone. The values shown were normalized to the average of those time points before treatment.
801 n = 4.

802

803 **Extended Data Table 1. All the primes used in this study**

804



805

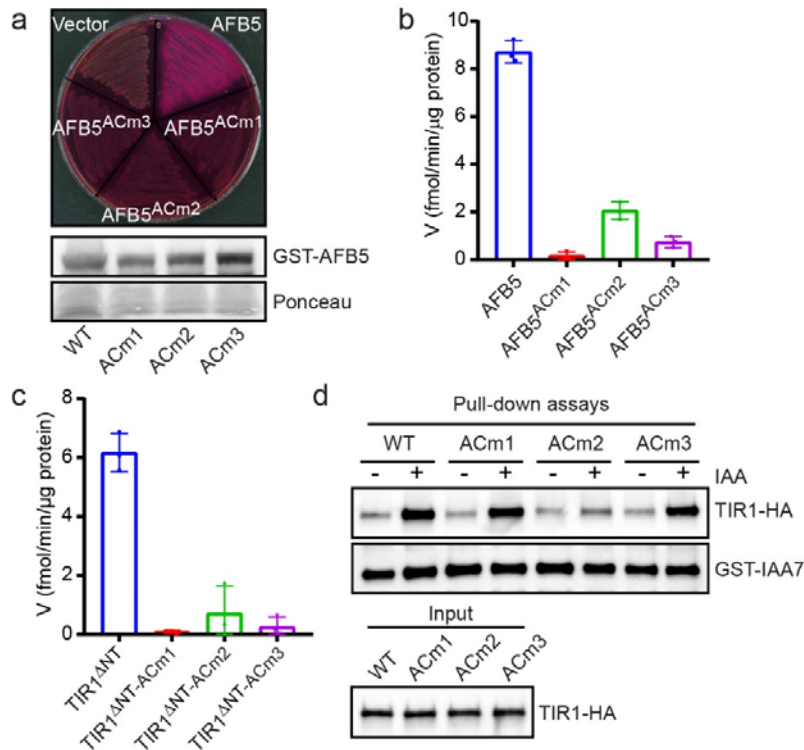
806 **Figure 1. TIR1/AFB auxin receptors have adenylate cyclase activity**

807 **a**, Alignment of the C-terminal protein sequences of TIR1/AFBs with the conserved AC motif.
 808 LRR, leucine-rich repeat. The residues m1-m3 indicate the conserved key amino acids, which
 809 were mutated to alanine to disrupt the AC activity (shown in Fig. 2).

810 **b-d**, *in vitro* AC activity of GST-**AFB5** purified from *E.coli*. AC activity assay in the presence
 811 of 2 different co-factors, followed by cAMP quantification by EIA (Enzyme ImmunoAssay)
 812 kit. The values shown were blanked against the background signals from the corresponding
 813 GST samples (**b**). Typical LC-MS/MS spectrum showing cAMP detection in the AC reaction
 814 with the characteristic peak used for quantification (**c**). Michaelis-Menten kinetics for the AC
 815 activity quantified by LC-MS/MS. S, substrate; V, velocity (**d**). For each data point, means \pm
 816 SD from 3 biological replicates are shown.

817 **e**, *in vitro* AC activity of His-GFP-FLAG-TIR1 purified from *Sf9* insect cells. Michaelis-
 818 Menten kinetics giving results similar to GST-**AFB5** (shown in d).

819



820

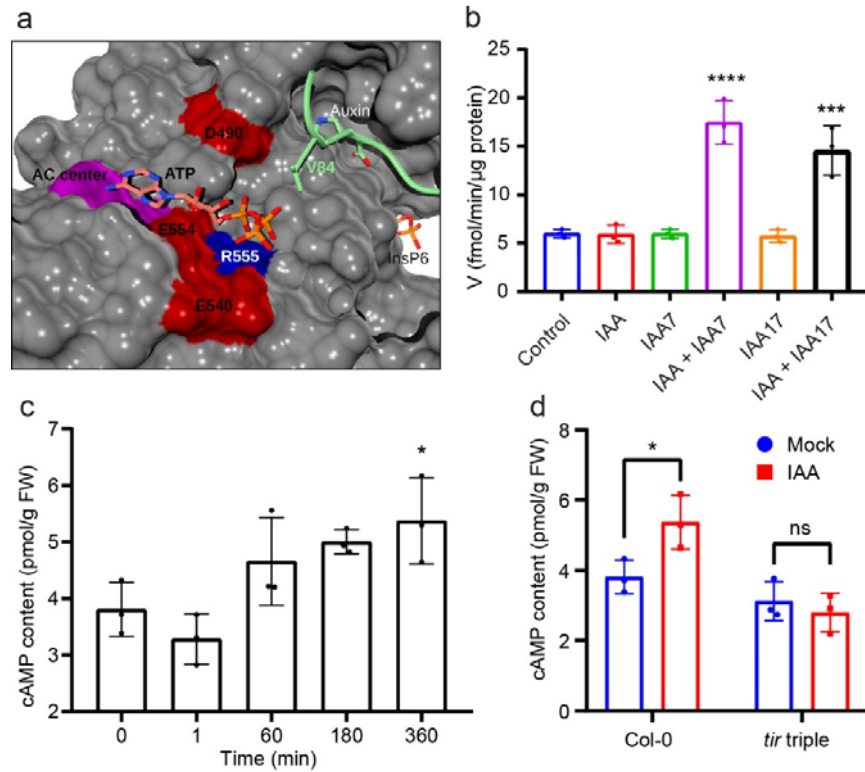
821 **Figure 2. C-terminal AC motif is responsible for the TIR1/AFB AC activity**

822 **a-b**, C-terminal AC motif is essential for the AFB5 AC activity. The AC deficient *E. coli* strain
 823 SP850 was complemented by the indicated constructs. The red colour of the MacConkey agar
 824 indicates the presence of AC activity. The empty vector *pGEX-4T-1* was used as negative
 825 control. Western blot confirms similar expression levels of endogenous and mutated AFB5
 826 proteins. Ponceau staining of the membrane was used as the loading control (**a**). *in vitro* AC
 827 activity assay for the purified GST-AFB5 and 3 mutated variants, followed by the cAMP
 828 quantification using LC-MS/MS. V, velocity. The values shown are means \pm SD from 3
 829 biological replicates (**b**).

830 **c**, C-terminal AC motif is essential for the AC activity of TIR1^{ΔNT}. GST-TIR1^{ΔNT} and 3
 831 mutated variants were purified from *E. coli*. An *in vitro* AC activity assay was performed
 832 followed by cAMP quantification using LC-MS/MS. V, velocity. The values shown are means
 833 \pm SD from 3 biological replicates.

834 **d**, Pull-down results showing differential effects of TIR1^{ACm} mutations on the IAA-induced
835 TIR1-Aux/IAA interaction. Wild-type and the 3 mutated TIR1 variants were translated *in vitro*
836 using wheat germ extracts, and were then used for pull-down assays with purified GST-IAA7,
837 in the presence or absence of 10 μ M IAA as indicated.

838



839

840 **Figure 3. Auxin perception enhances the TIR1/AFBs AC activity**

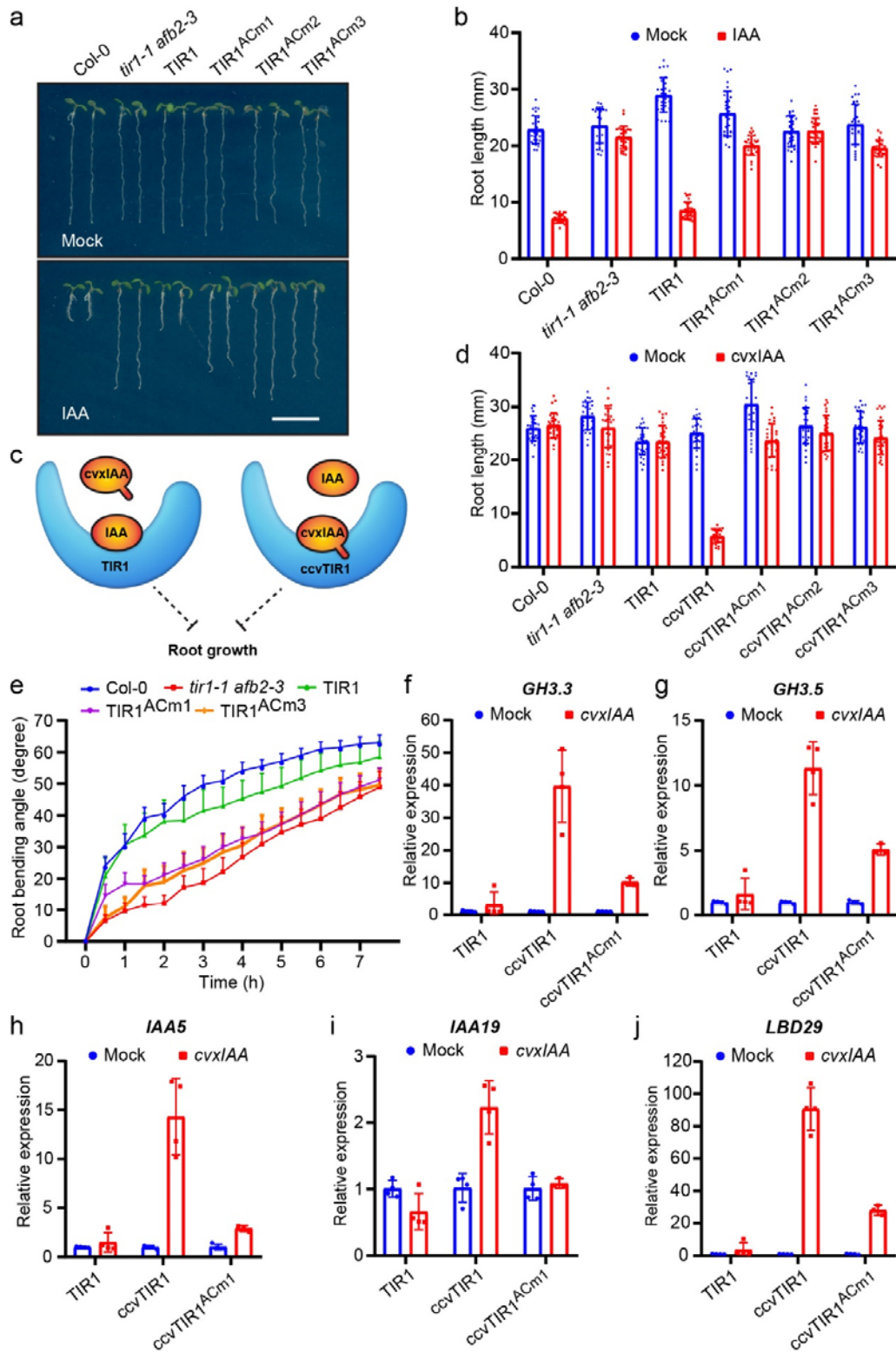
841 **a**, Docking of ATP on the surface of TIR1-IAA-Aux/IAA complex. The beginning of the AC
 842 center was labelled in magenta. Amino acids presumably important for the AC activity were
 843 labelled either in red (acidic), or in blue (basic). E554 is the site for m1 (as in Fig. 1a). Note
 844 that V84 from the Aux/IAA degron restricts the space available to ATP.

845 **b**, Auxin together with Aux/IAA stimulates the TIR1 AC activity. *in vitro* AC activity assay
 846 with His-GFP-FLAG-TIR1 (5 μg) in the presence of 10 μM IAA, IAA7 (3 μg), IAA17 (3 μg)
 847 and the indicated combinations, followed by cAMP quantification using LC-MS/MS. V,
 848 velocity. One-way ANOVA. n = 3. *** p ≤ 0.001; **** p ≤ 0.0001.

849 **c**, Auxin treatment increases cAMP content in root tissues. Five-days-old Col-0 seedlings were
 850 treated with 100 nM IAA. Root tissues were harvested for cAMP quantification by LC-MS/MS.
 851 One-way ANOVA. n = 3. * p ≤ 0.05.

852 **d**, Auxin-induced increase of cAMP levels in roots is dependent on TIR1/AFBs. Five-days-old
853 Col-0 or *tir* triple seedlings were treated with 100 nM IAA for 6 h. Root tissues were collected
854 for cAMP measurement by LC-MS/MS. One-way ANOVA. n = 3. * $p \leq 0.05$. ns, not
855 significant.

856



857

858 **Figure 4. TIR1 AC activity contributes to auxin-induced root growth inhibition and**

859 **transcriptional responses**

860 **a-b**, AC motif mutations compromise TIR1 function in mediating IAA-induced root growth
861 inhibition. *pTIR1::TIR1* and the similar constructs containing the 3 AC motif mutations were
862 transformed into *tir1-1afb2-3*. Representative examples of 6-days-old seedlings of different
863 genotypes grown on Mock or 100 nM IAA containing medium. Bar = 10 mm (**a**).
864 Quantification of the root length in (a). n = 30 (**b**).

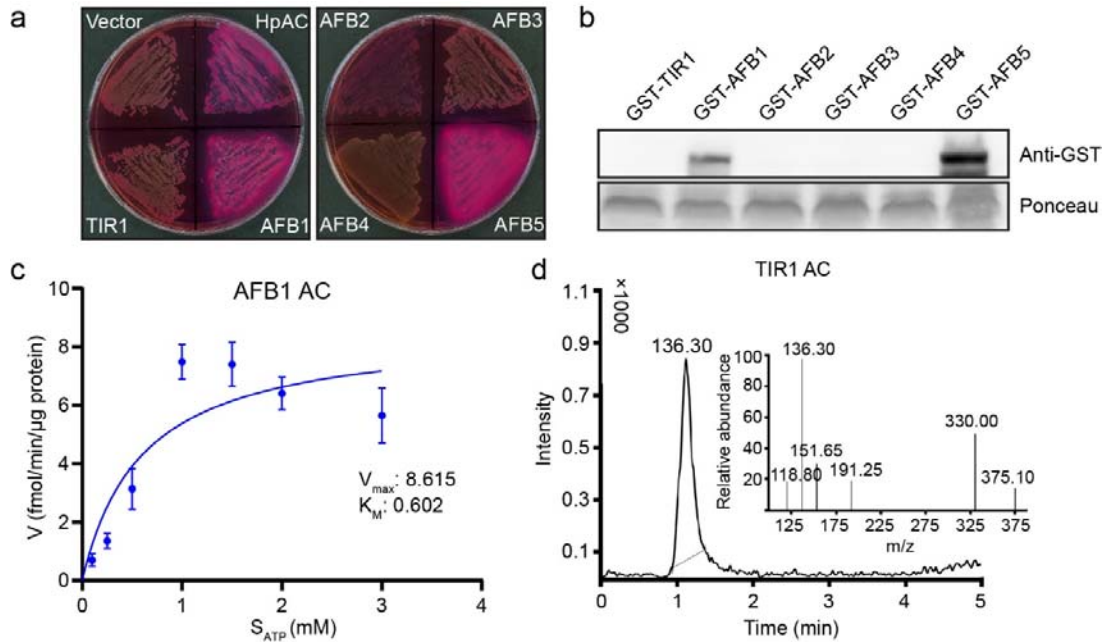
865 **c**, Simplified scheme showing the principles of the engineered cvxIAA/ccvTIR1 system.

866 **d**, C-terminal AC motif is crucial for cvxIAA-triggered root growth inhibition in *ccvTIR1* line.
867 *pTIR1::TIR1*, *pTIR1::ccvTIR1*, and the 3 similar constructs containing the AC motif mutations
868 (see Fig. 1a) were transformed into *tir1-1afb2-3*. Root length of the 6-days-old seedlings with
869 different genotypes grown on Mock or 500 nM cvxIAA containing medium were measured. n
870 = 30.

871 **e**, AC activity is required for TIR1 function in root gravitropism. Five-days-old seedlings of
872 the indicated genotypes were transferred to new plates. The plates were rotated 90 degree
873 before images were captured every 30 min. Root bending angle was measured to monitor the
874 gravitropic response. n = 10.

875 **f-j**, AC activity contributes to auxin-induced genes expression. Five-days-old seedlings were
876 either Mock-treated or treated with liquid medium containing 200 nM cvxIAA for 3 h.
877 Seedlings were harvested for RNA extraction and qRT-PCR. Shown are the relative expression
878 values normalized to the internal control *PP2AA3*, from 3 or 4 biological replicates.

879



880

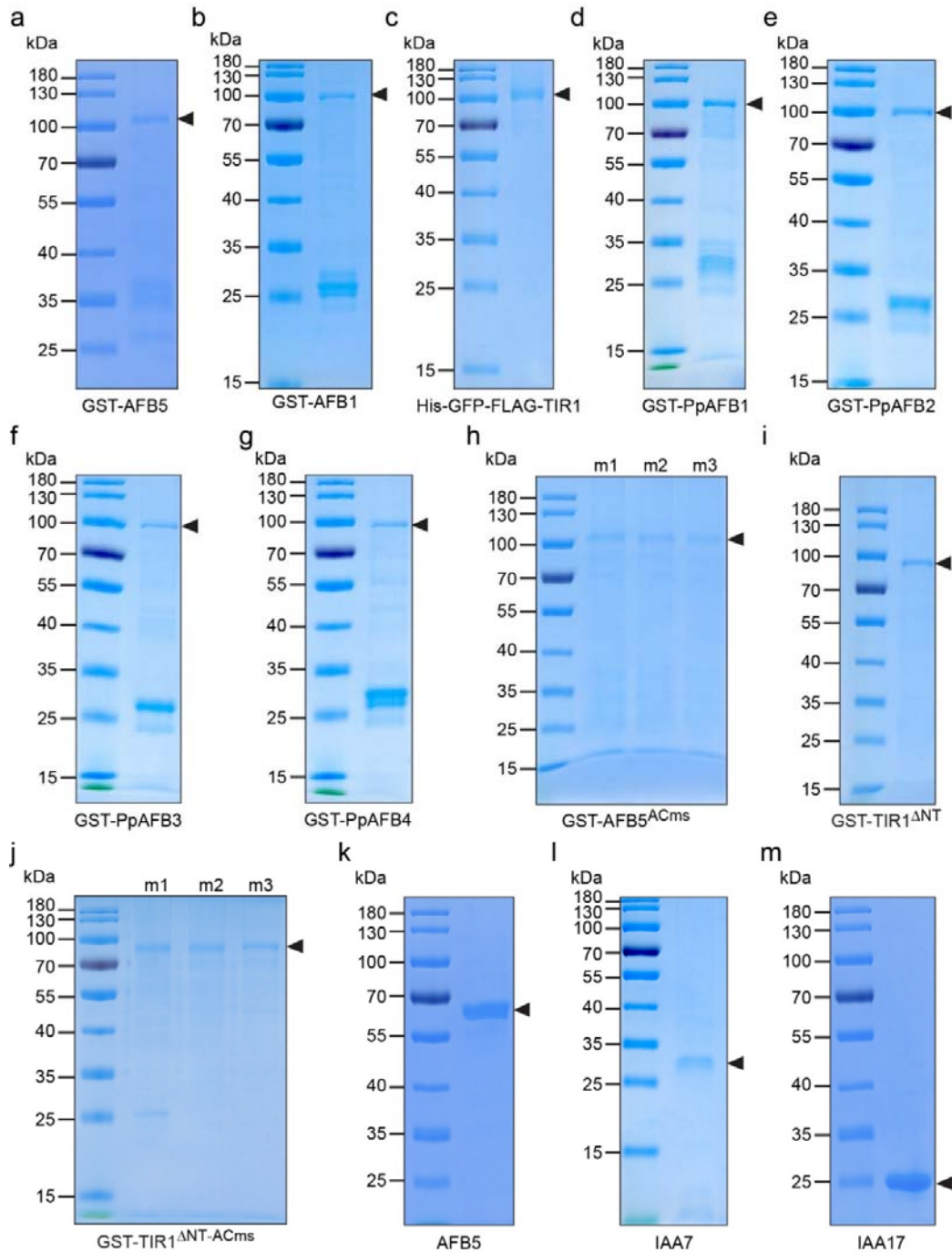
881 **Extended Data Figure 1. Additional data to support the AC activity of TIR1/AFBs**

882 **a-b**, *E. coli* complementation assay showing that AFB1 and AFB5 have AC activity. The AC
 883 deficient SP850 strain was complemented with the empty vector (*pGEX-4T-1*), the positive
 884 control (HpAC1), and TIR1/AFBs. Red colour of the MacConkey Agar indicates the presence
 885 of AC activity (a). Western blot result shows that only AFB1 and AFB5 can be visibly detected
 886 among the 6 members of TIR1/AFBs. Ponceau red staining of the membrane was used as the
 887 loading control.

888 **c**, Michaelis-Menten kinetics for the AC activity of GST-AFB1 purified from *E. coli*. cAMP
 889 level after reaction was quantified by LC-MS/MS. S, substrate; V, velocity. For each data point,
 890 means \pm SD from 3 biological replicates are shown.

891 **d**, Representative LC-MS/MS spectrum showing the detection of cAMP after the *in vitro* AC
 892 activity assay for His-GFP-FLAG-TIR1 purified from *Sf9* insect cells.

893



894

895 **Extended Data Figure 2. Gel images showing the purity of all the proteins used**

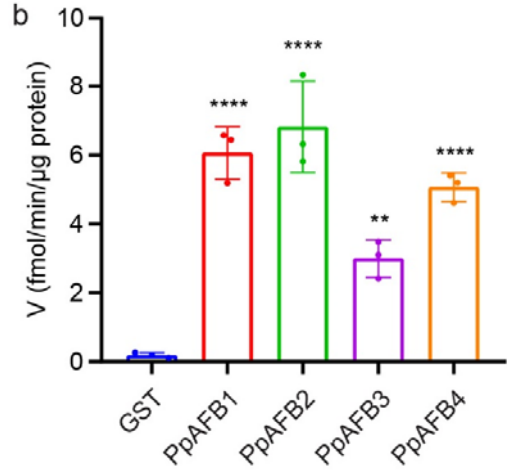
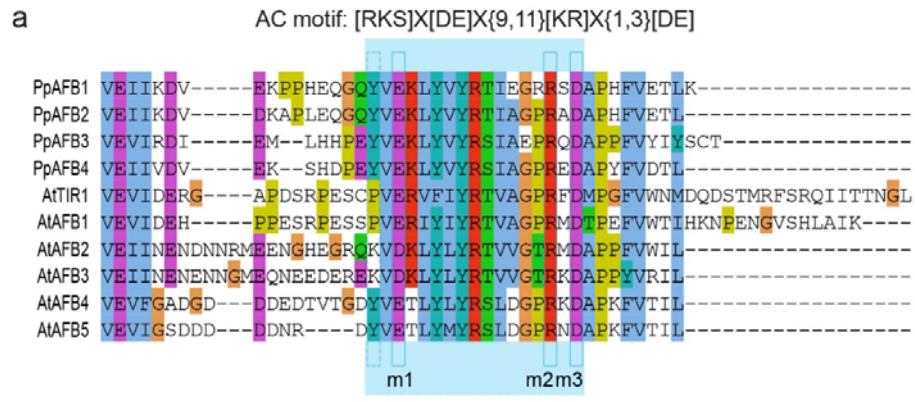
896 **a, GST-AFB5. b, GST-AFB1. c, His-GFP-FLAG-TIR1. d, GST-PpAFB1. e, GST-PpAFB2. f,**

897 **GST-PpAFB3. g, GST-PpAFB4. h, GST-AFB5^{ACm1/m2/m3}. i, GST-TIR1^{ΔNT}. j, GST-TIR1^{ΔNT}-**

898 **ACm1/m2/m3. k, AFB5 after cleavage of GST tag. l, IAA7 after cleavage of GST tag. m, IAA17**

899 after cleavage of GST tag. His-GFP-FLAG-TIR1 was purified from *Sf9* insect cells. All the
900 other proteins were purified from BL-21 *E. coli* cells. Proteins were separated on SDS-PAGE
901 gels and the gels were stained with Coomassie Brilliant Blue.

902



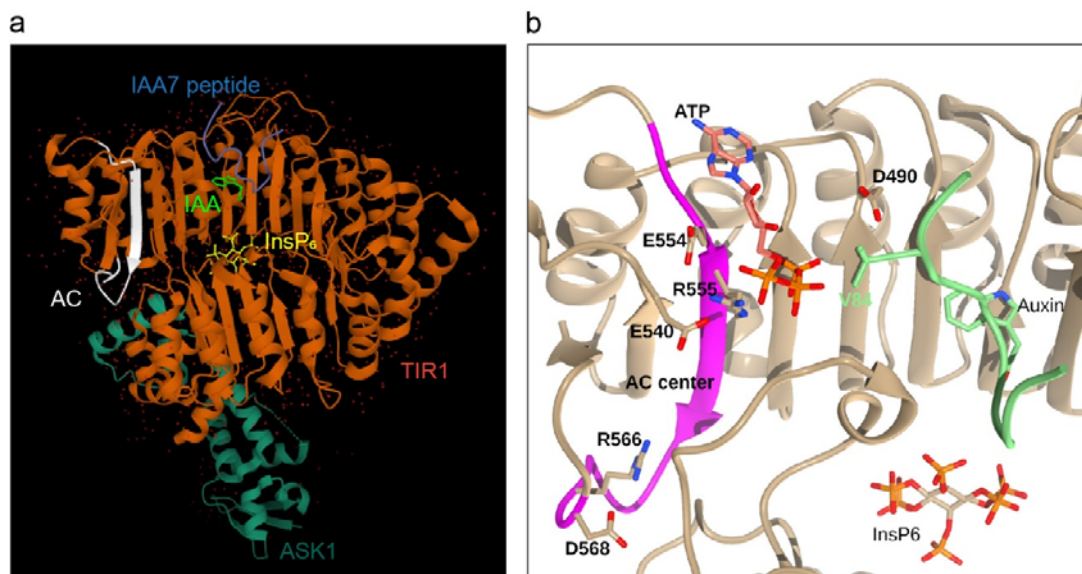
903

904 **Extended Data Figure 3. AC activity is conserved in TIR1/AFBs orthologues from**
905 ***Physcomitrella***

906 **a**, Alignment of the C-terminal protein sequences of TIR1/AFBs together with their
907 orthologues from *Physcomitrella*. Note the AC motif is highly conserved in all the sequences.
908 Only the first amino acid is a bit more relaxed.

909 **b**, TIR1/AFBs orthologues from *Physcomitrella* have AC activity. GST-tagged PpAFBs were
910 purified from *E. coli*. *in vitro* AC activity assay was performed with GST as the negative
911 control. cAMP level after reaction was quantified using LC-MS/MS. The values shown are
912 means ± SD from 3 biological replicates. One-way ANOVA. ** $p \leq 0.01$; **** $p \leq 0.0001$.

913



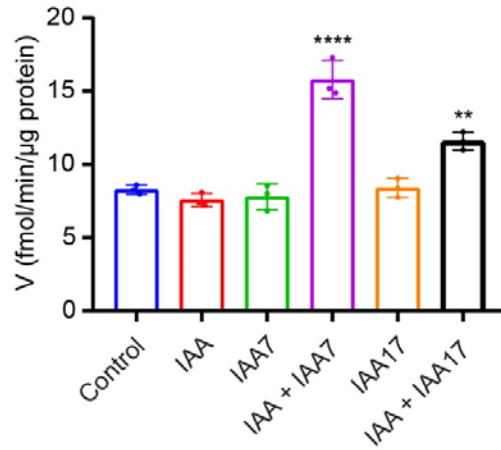
914

915 **Extended Data Figure 4. Protein structure of TIR1-IAA-Aux/IAA complex and ribbon**
 916 **structure showing ATP docking**

917 **a**, Protein structure of TIR1-IAA-Aux/IAA complex showing the spatial position of the C-
 918 terminal AC motif. Different parts were labelled as different colours. Dark green, ASK1; Red,
 919 TIR1; White, C-terminal AC motif; Blue, IAA7 peptide; Yellow, InsP₆ (inositol
 920 hexakisphosphate); Green, IAA.

921 **b**, Ribbon structure showing the interaction of ATP with the key amino acids of the AC motif.
 922 AC center was labelled in magenta. E554 is the residue identified for m1 in Fig. 1a, R566 for
 923 m2, and D568 for m3. Note that V84 from the Aux/IAA degron restricts the space available to
 924 ATP.

925

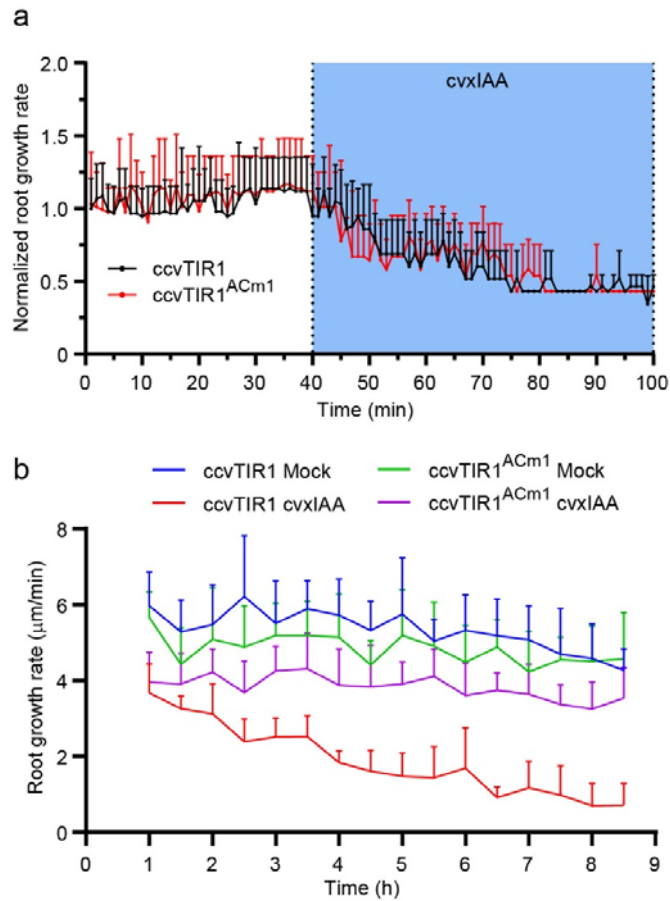


926

927 **Extended Data Figure 5. Auxin perception enhances the AC activity of AFB5**

928 *in vitro* AC activity assay for AFB5 in the presence of 10 μM IAA, IAA7, IAA17 and the
 929 indicated combinations, followed by cAMP quantification using LC-MS/MS. Tag-cleaved
 930 clean proteins were used for this experiment. One-way ANOVA. n = 3. ** $p \leq 0.01$; **** $p \leq$
 931 0.0001.

932



933

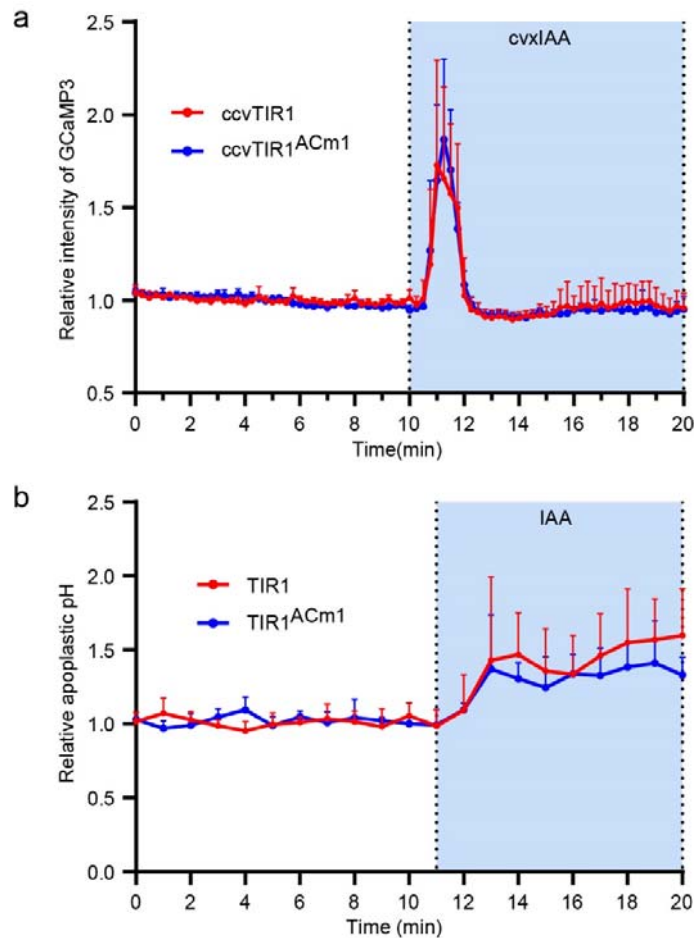
934 **Extended Data Figure 6. Delayed requirement of the AC activity in root growth**
 935 **regulation**

936 **a**, Loss of AC activity does not affect cvxIAA/ccvTIR1-induced root growth inhibition within
 937 the first hour. A vRootchip experiment was performed with the transgenic lines indicated, and
 938 the images were captured with a time interval of 1 min. Mock medium was changed to medium
 939 containing 500 nM of cvxIAA at 40 min. Root growth rate was normalized to the starting point
 940 of the respective group. n = 4.

941 **b**, Resistance of ccvTIR1^{ACm1} to cvxIAA-triggered root growth inhibition occurs only after 1
 942 h of treatment. Vertical scanner growth assay was performed to track the root growth dynamics.
 943 Five-days-old seedlings of the indicated genotypes were transferred to either Mock medium or

944 medium containing 200 nM of cvxIAA. Images were taken every 30 min. Root growth rate
945 was measured. n = 10.

946



947

948 **Extended Data Figure 7. TIR1 AC activity is not crucial for rapid auxin responses**

949 **a**, cvxIAA triggers similar Ca²⁺ spikes in the *ccvTIR1* and *ccvTIR1^{ACm1}* lines. The calcium
 950 sensor GCaMP3 was crossed to the indicated transgenic lines. Five-days-old F1 seedlings were
 951 used for vRootchip experiment, and the images were captured with a time interval of 15 s.
 952 Mock medium was changed to medium containing 500 nM of cvxIAA at 10 min. The
 953 fluorescence signal in the epidermal cells of root elongation zone was quantified, and was
 954 normalized to the average value of time points before treatment. n = 4.

955 **b**, Auxin-induced apoplastic alkalinisation is not changed in the *TIR1^{ACm1}* line. Five-days-old
 956 seedlings of the indicated genotypes were used for vRootchip experiment. Mock medium was
 957 changed to medium containing 10 nM of IAA at 11 min. Ratiometric (488 nm/405nm) imaging

958 of HPST staining was used to measure apoplastic pH in the epidermal cells of root elongation
959 zone. The values shown were normalized to the average of those time points before treatment.
960 n = 4.

961

962 **Extended Data Table 1. All the primes used in this study**

| Primers | Sequences | Usage |
|----------------------|--|--------------------------------------|
| <i>tir1-1</i> -GT-FP | AGCGACGGTGATTAGGAGGT (CAPS, digestion with Bsa I) | Genotyping |
| <i>tir1-1</i> -GT-RP | CAGGAACAACGCAGCAAAA | |
| <i>afb2-3</i> -GT-FP | TTCTCCTTCGATCATTGTCAAC | |
| <i>afb2-3</i> -GT-RP | TAGCGGCAATAGAGGCAAGA | |
| LBB1.3 | ATTTTGCCGATTTCGGAAC (for SALK lines) | |
| TIR1-pGEX-FP | CGC GGATCC ATGCAGAAGCGAATAGCCTTG (BamHI) | Protein expression in <i>E. coli</i> |
| TIR1-pGEX-RP | ACGC GTCGAC TTATAATCCGTTAGTAGTAATGATTG GCC (Sall) | |
| AFB1-pGEX-FP | CGC GGATCC ATGGGTCTCCGATTCCCACCT (BamHI) | |
| AFB1-pGEX-RP | ACGC GTCGAC TTACTTTATGGCTAGATGTGAAA CTCCATTC (Sall) | |
| AFB2-pGEX-FP | CGC GGATCC ATGAATTATTTCCCAGATGAAGTA ATAGAG (BamHI) | |
| AFB2-pGEX-RP | ACGC GTCGAC TTAGAGAATCCACACAAATGGC G (Sall) | |
| AFB3-pGEX-FP | CGC GGATCC ATGAATTATTTCCCAGACGAGGTT (BamHI) | |
| AFB3-pGEX-RP | ACGC GTCGAC CTAAAGAATCCTAACATATGGTG GTG (Sall) | |
| AFB4-pGEX-FP | CGC GGATCC ATGACAGAAGAAGATAGCTCAGC (BamHI) | |
| AFB4-pGEX-RP | ACGC GTCGAC TCATAAAATTGTTACAACTTTG GAGC (Sall) | |
| AFB5-pGEX-FP | CGC GGATCC ATGACACAAGATCGCTCAGAAAT G (BamHI) | |
| AFB5-pGEX-RP | CCG CTCGAG CTATAAAATCGTGACGAACTTTGG T (XhoI) | |
| TIR1 ΔNT - pGEX-FP | CGC GGATCC CCTTGAAGAGATAAGGCTGAAGAG GA (BamHI) | |
| IAA7-pGEX-FP | CGC GGATCC ATGATCGGCCAACTTATGAACC (BamHI) | |

| | | |
|---------------|---|-------------------------------|
| IAA7-pGEX-RP | ACGC <u>GTCGACT</u> TCAAGATCTGTTCTTGCAGTACT TCTC (Sall) | |
| IAA17-pGEX-FP | CGC <u>GGATCC</u> ATGATGGGCAGTGTCGAGCTG (BamHI) | |
| IAA17-pGEX-RP | CCG <u>CTCGAG</u> TCAAGCTCTGCTCTTGCACCTTCTC (XhoI) | |
| TIR1p-B4-FP | <u>GGGGACAACCTTTGTATAGAAAAGTTG</u> AGGCT AAAAATAAATGCGGAAAAAAG (AttB4) | Transgenic plants |
| TIR1p-B1r-RP | <u>GGGGACTGCTTTTTGTACAAACTTG</u> TGCGGC CAAATAACCTCGAG (AttB1r) | |
| TIR1-B1-FP | <u>GGGGACAAGTTTGTACAAAAAAGCAGGCTTCA</u> TGCAGAAGCGAATAGCCTTG (AttB1) | |
| TIR1-B2-RP | <u>GGGGACCACTTTGTACAAGAAAGCTGGGT</u> TTTA TAATCCGTTAGTAGTAATGATTTGCC (AttB2) | |
| TIR1-ccv-FP | GAAACCTCACGGTGCTGACTTTAATTTG | ccvTIR1 mutation |
| TIR1-ccv-RP | CTTAAGCTCCACGGATCTCACTTTC | |
| TIR1-ACm1-FP | CTGCCCTGTTGCGAGAGTCTTCATATAC | TIR1 AC motif mutations |
| TIR1-ACm1-RP | CTCTCTGGTCTCGAGTCCGGTG | |
| TIR1-ACm2-FP | TGGCTGGTCTGCATTTGACATGC | |
| TIR1-ACm2-RP | CTGTTGCGGTATATGAAGACTCTCTCAACAG | |
| TIR1-ACm3-FP | TCCTCGATTTGCCATGCCTGGCT | |
| TIR1-ACm3-RP | CCAGCCACTGTTCCGGTATATGAAGAC | |
| AFB5-ACm1-FP | AGGGATTATGTCGCTACTTTATACATGTATC | AFB5 AC motif mutations |
| AFB5-ACm1-RP | ATTGTCATCATCATCATCCGATCC | |
| AFB5-ACm2-FP | CTTGATGGTCCAGCTAATGATGCACC | |
| AFB5-ACm2-RP | AGACCGATACATGTATAAAGTCTCGAC | |
| AFB5-ACm3-FP | GTCCAAGGAATGCTGCACCAAAGTTC | |
| AFB5-ACm3-RP | CATCAAGAGACCGATACATGTATAAAGTC | |
| pGEX-S-F | GGGCTGGCAAGCCACGTTTGGTG | Sequencing |
| pGEX-S-R | CCGGGAGCTGCATGTGTCAGAGG | |
| TIR1p-S-F1 | CCACACTTCTCCCATCTGACTAT | |
| M13-21F | TGTAACGACGACGGCCAGT | |
| M13-29R | CAGGAAACAGCTATGACC | |
| PP2AA3-q-FP | TAACGTGGCCAAAATGATGC | qRT-PCR |
| PP2AA3-q-RP | GTTCTCCACAACCGCTTGGT | |
| GH3.3-q-FP | CATCACAGAGTTCCTCACAAGC | |
| GH3.3-q-RP | GTCGGTCCATGTCTTCATCA | |

| | | |
|------------|---------------------------|--|
| GH3.5-q-FP | CATCTCTGAGTTCCTCACAAGC | |
| GH3.5-q-RP | CCTCTTCGATTGTTGGCATT | |
| IAA5-q-FP | TGAAGGAAAGTGAATGTGTACCAA | |
| IAA5-q-RP | GCACGATCCAAGGAACATT | |
| IAA19-q-FP | TGGTGACAACCTGCGAATACGTTAC | |
| IAA19-q-RP | CGTCTACTCCTCTAGGCTGCAG | |
| LBD29-q-FP | GCTAGGCTTCAAGATCCCATC | |
| LBD29-q-RP | TGTGCTGCTTGTTGCTTTAGA | |

963

964

965